MCL-1 is a master regulator of cancer dependency on fatty acid oxidation

Michelle S. Prew[1], **Utsarga Adhikary**[1], **Dong Wook Choi**[2,3], **Erika P. Portero**[2,3], **Joao A. Paulo**[3], **Pruthvi Gowda**[2,3], **Amit Budhraja**[4], **Joseph T. Opferman**[4], **Steven P. Gygi**[3], **Nika N. Danial**[2,3], **Loren D. Walensky**[1,5,*]

[1]Department of Pediatric Oncology and Linde Program in Cancer Chemical Biology, Dana-Farber Cancer Institute, Boston, MA 02215, USA

[2]Department of Cancer Biology, Dana-Farber Cancer Institute, Boston, MA 02215, USA

[3]Department of Cell Biology, Harvard Medical School, Boston, MA 02115, USA

[4]Department of Cell and Molecular Biology, St. Jude Children's Research Hospital, Memphis, TN 38105, USA

[5]Lead contact

SUMMARY

MCL-1 is an anti-apoptotic BCL-2 family protein essential for survival of diverse cell types and is a major driver of cancer and chemoresistance. The mechanistic basis for the oncogenic supremacy of MCL-1 among its anti-apoptotic homologs is unclear and implicates physiologic roles of MCL-1 beyond apoptotic suppression. Here we find that MCL-1-dependent hematologic cancer cells specifically rely on fatty acid oxidation (FAO) as a fuel source because of metabolic wiring enforced by MCL-1 itself. We demonstrate that FAO regulation by MCL-1 is independent of its anti-apoptotic activity, based on metabolomic, proteomic, and genomic profiling of MCL-1-dependent leukemia cells lacking an intact apoptotic pathway. Genetic deletion of *Mcl-1* results in transcriptional downregulation of FAO pathway proteins such that glucose withdrawal triggers cell death despite apoptotic blockade. Our data reveal that MCL-1 is a master regulator of FAO, rendering MCL-1-driven cancer cells uniquely susceptible to treatment with FAO inhibitors.

*Correspondence: loren_walensky@dfci.harvard.edu.

Graphical abstract

In brief

Prew et al. report that, independent of its anti-apoptotic function, MCL-1 enforces a programmatic dependency on fatty acid oxidation (FAO) in MCL-1-driven hematologic cancer cells, rendering them vulnerable to FAO inhibition. *Mcl-1* deletion broadly downregulates the FAO pathway, revealing MCL-1 as a master regulator of fatty acid metabolism.

INTRODUCTION

Mitochondrial apoptosis is an essential physiologic process that eliminates damaged or unwanted cells during development and homeostasis (Danial and Korsmeyer, 2004). BCL-2 family proteins regulate apoptosis through a protein interaction network composed of pro- and anti-apoptotic members. Pro-apoptotic BAX and BAK are executioner proteins that, when triggered, transform from latent monomers into toxic oligomers that permeabilize the mitochondrial outer membrane, releasing signaling factors, such as cytochrome *c*, that drive the caspase cascade and subsequent cellular self-destruction (Farrow et al., 1995; Liu et al., 1996; Oltvai et al., 1993). The anti-apoptotic members, such as BCL-2 and MCL-1, can arrest the apoptotic process by trapping activated monomers of BAX/BAK through heterodimeric interaction, preventing mitochondrial damage (Czabotar et al., 2014; Sattler et al., 1997). An additional layer of regulation is provided by the BH3-only proteins, which serve as afferent sensors of cellular stress and deliver pro-apoptotic signals to the core pro-

and anti-apoptotic members (Wei et al., 2000). When BH3-only signaling overwhelms the anti-apoptotic reserve, latent monomers of BAX and BAK can become directly activated by select BH3-only members and indirectly activated by competitive displacement from anti-apoptotic proteins (Walensky and Gavathiotis, 2011). Deregulation of BCL-2 family interactions can disrupt the delicate balance between cellular life and death, causing diseases of cellular excess or deficiency (Rinkenberger and Korsmeyer, 1997).

MCL-1 is an anti-apoptotic BCL-2 protein with distinguishing features. It is a much larger protein than its counterparts, featuring an N-terminal extension of unknown function (Reynolds et al., 1994). Global and conditional deletion of *Mcl-1* have uniquely profound physiologic consequences, including embryonic lethality (Rinkenberger et al., 2000), immune deregulation (Opferman et al., 2003), hematopoietic stem cell loss (Opferman et al., 2005), and fatal cardiomyopathy (Wang et al., 2013). The inability of anti-apoptotic homologs to compensate for *Mcl-1* deletion in these contexts suggests that MCL-1 may have broader roles in organism homeostasis beyond apoptotic suppression. MCL-1 is among the most highly overexpressed pathologic proteins across all human cancers (Beroukhim et al., 2010) and is linked to poor prognoses, chemotherapy resistance, and relapse (Wei et al., 2006; Wuillème-Toumi et al., 2005). Thus, therapeutic targeting of MCL-1 in cancer is a high-priority goal. Although clinical testing of candidate small-molecule inhibitors of MCL-1 is underway, emerging toxicities beyond what has been observed with selective BCL-2 inhibition (Roberts et al., 2016) have halted several trials (Wang et al., 2021), again suggesting that MCL-1 targeting may have physiological consequences beyond suppression of anti-apoptotic activity.

Consistent with their mitochondrial localization, select BCL-2 proteins regulate mitochondrial morphology (Karbowski et al., 2006) and specific metabolic enzymes (Danial et al., 2003; Gimenez-Cassina and Danial, 2015). Recent studies have implicated MCL-1 in these homeostatic processes. A mitochondrial matrix-localized isoform of MCL-1 (MCL-1^{Matrix}) is required for maintenance of mitochondrial ultrastructure and cristae morphology and for the functional assembly of electron transport chain super-complexes and higher-order ATP synthase complexes (Huang and Yang-Yen, 2010; Perciavalle et al., 2012). While pursuing proteomic analyses to identify potential targets of MCL-1 in the mitochondrial matrix, we discovered that the BH3 helix of MCL-1 directly interacts with very long-chain acylcoenzyme A (CoA) dehydrogenase (VLCAD), an enzyme that catalyzes the first step of the long-chain fatty acid oxidation (FAO) pathway (Escudero et al., 2018). Selective loss of MCL-1^{Matrix} causes deregulation of FAO, as reflected by accumulation of long-chain acylcarnitines in mouse embryonic fibroblasts and murine liver (Escudero et al., 2018).

Although we initially established a link between MCL-1 and fatty acid metabolism in normal cells and tissue, we subsequently explored the potential relevance to cancer, given that deregulation of cellular metabolism is a major hallmark of human cancer (Hanahan and Weinberg, 2011; Vander Heiden and DeBerardinis, 2017). Gene set enrichment analyses revealed a statistically significant correlation between elevated *MCL-1* expression and an FAO signature across two independent datasets containing 524 and 294 cases of human acute myeloid leukemia (AML); no such correlation was observed for anti-apoptotic *BCL-*

X_L expression, for example (Escudero et al., 2018). Reliance on FAO for cancer cell survival, proliferation, and metastasis has emerged as a prominent outcome of metabolic reprogramming in cancer (Carracedo et al., 2013; Ma et al., 2018; Snaebjornsson et al., 2020), including in the context of resistance to the selective BCL-2 inhibitor venetoclax (Stevens et al., 2020), where MCL-1 typically plays a role (Yecies et al., 2010). Understanding how MCL-1 may contribute to this FAO phenotype is not only essential for elucidating fundamental MCL-1 biology but also for developing safe and effective treatment strategies that target MCL-1-dependent cancers and overcome MCL-1-mediated chemoresistance.

RESULTS

MCL-1 regulates metabolism independent of its anti-apoptotic function

A key challenge in delineating non-canonical roles for MCL-1 in biology is the confounding effect of its established function as a suppressor of mitochondrial apoptosis. To definitively dissociate MCL-1's anti-apoptotic activity from its potential role as a metabolic regulator, we took advantage of MCL-1-dependent murine p185$^+$Arf$^{-/-}$ B-cell acute lymphoblastic leukemia (B-ALL) cells (Koss et al., 2013, 2016; Lee et al., 2019) lacking either BAX and BAK (p185$^+$Arf$^{-/-}$Bax$^{-/-}$Bak$^{-/-}$) or BAX, BAK, and MCL-1 (p185$^+$Arf$^{-/-}$Bax$^{-/-}$Bak$^{-/-}$Mcl-1$^{-/-}$), hereafter referred to as double knock-out (DKO) and triple knock-out (TKO) cells, respectively (Figure 1A). We first examined whether cells lacking MCL-1 could respond to metabolic stress, such as glucose deprivation, which typically triggers a switch from glucose to fatty acid utilization (Raulien et al., 2017). In the absence of BAX/BAK-mediated mitochondrial apoptosis, DKO cells remained fully viable in regular and low-glucose media; however, genetic deletion of *Mcl-1* resulted in a dramatic loss of viability under low-glucose conditions (Figure 1B). This striking vulnerability of TKO cells was rescued by providing alternate sources of acetyl-CoA for the tricarboxylic acid cycle (TCA) cycle, such as pyruvate or acetate, indicative of a specific metabolic lesion (Figure 1C). The inability to compensate for glucose deprivation by switching to FAO as a fuel source could underlie the observed cell death, which notably occurred in the absence of BAX and BAK. Compared with the normal appearance of DKO cells cultured in regular and low-glucose media (Figures 1D and 1E), electron microscopy revealed prominent vacuolization and autophagocytosis of TKO cells when subjected to the low-glucose condition (Figures 1F–1I), consistent with non-apoptotic cell death in response to glucose deprivation.

Mcl-1 deletion shifts cellular fuel usage from lipids to glucose

To characterize the metabolic changes arising from loss of MCL-1, we measured the oxygen consumption rate (OCR) in DKO and TKO cells by Seahorse analysis, performed in the presence and absence of added palmitate. Although DKO cells demonstrated an increased OCR in response to added palmitate (Figure 1J), TKO cells showed no such effect (Figure 1K), consistent with a defect in palmitate utilization. To further characterize this finding, we performed metabolite tracing experiments. For FAO analysis, DKO and TKO cells were grown in regular or low-glucose medium containing uniformly labeled ^{13}C-palmitate (U^{13}C-palmitate), and relative levels of citrate labeled on two carbons (M+2 citrate) were

measured as a readout of FAO (Caro et al., 2012; Figure 2A). In regular medium, the percentage of M+2 citrate detected in DKO cells was more than double that of TKO cells; in low-glucose medium, the difference between cell types was even more dramatic, with DKO cells demonstrating increased FAO compared with TKO cells, which exhibited a blunted response (Figure 2B). Thus, DKO cells adapt to a low-glucose environment by increasing palmitate utilization, whereas TKO cells demonstrate not only a baseline reduction in FAO but also an inability to adequately upregulate long-chain fatty acid utilization in response to the stress of glucose deprivation. These data provide a mechanistic explanation for the non-apoptotic cell death observed in TKO cells when cultured in low-glucose medium (Figure 1B). To determine whether the metabolic defect in TKO cells was selective for long-chain FAO, we repeated the analysis using 1^{13}C-hexanoate in regular medium and likewise observed a statistically significant difference in short-chain FAO between DKO and TKO cells (Figure S1). Although less dramatic of a defect than observed for long-chain FAO in TKO cells, these data suggest that MCL-1 regulation of FAO may extend beyond focal modulation of VLCAD by MCL-1[Matrix] (Escudero et al., 2018).

Given the difference in response of DKO and TKO cells to glucose deprivation, we next conducted U^{13}C-glucose tracing studies to measure glucose utilization (Figure 2C). No statistically significant difference was observed in glucose uptake between DKO and TKO cells (Figure 2D). However, TKO cells demonstrated markedly increased ^{13}C incorporation into glycolytic and TCA cycle intermediates compared with DKO cells (Figure 2D). Our combined metabolic tracing and nutrient withdrawal studies indicate that MCL-1-dependent cells effectively utilize fatty acids as a fuel source but are defective in FAO upon *Mcl-1* deletion, resulting in dependence on glucose metabolism for cell survival.

Selective deficiency of fatty acid utilization upon *Mcl-1* deletion

To expand our investigation of altered fatty acid metabolism in the absence of MCL-1, we measured free fatty acid (FFA) levels in DKO and TKO B-ALL cells cultured in regular or low-glucose medium. In regular medium, DKO cells exhibited elevated FFA levels compared with TKO cells, potentially reflecting increased mobilization of FFAs to sustain their use in FAO (Figure 3A). In low-glucose medium, FFA levels sharply decreased in DKO cells, perhaps suggestive of increased consumption because of heightened metabolic demand. In contrast, FFA levels increased slightly in TKO cells subjected to glucose deprivation, which would be consistent with an inability to efficiently mobilize and consume FFAs despite the metabolic demand. In agreement with this scenario, the ratio of FFAs in regular versus low-glucose medium is predominantly greater than 1 for DKO cells but uniformly lower than 1 for TKO cells (Figure 3B). Overall, these data are consistent with the metabolic tracing studies that revealed (1) elevated FAO in DKO versus TKO cells at baseline and upon glucose deprivation (Figure 2B) and (2) increased glucose metabolism in TKO versus DKO cells (Figure 2D). In parallel studies, we also performed untargeted metabolomics analysis in cells cultured in regular medium to assess the broader spectrum of MCL-1-dependent changes in metabolite patterns. However, among 921 metabolites identified in this analysis, few if any differences in steady-state levels of metabolites between DKO and TKO cells were observed (Figure S2). Our data point to

altered fatty acid metabolism as a predominant metabolic feature arising from a loss of MCL-1 function that is unrelated to mitochondrial apoptosis.

Global downregulation of the FAO pathway upon *Mcl-1* deletion

To discern whether the defect in FAO upon *Mcl-1* deletion in the absence of an intact apoptotic pathway is a focal or programmatic signaling phenomenon, we performed comparative proteomics analyses of DKO and TKO B-ALL cells cultured in regular or low-glucose medium. When examining 34 core members of the FAO pathway, we observed significantly higher enrichment of FAO proteins in DKO versus TKO cells when cultured in regular medium (Figures 3C and 3D). Glucose deprivation led to increased FAO protein levels in both contexts, with overall levels remaining higher in DKO versus TKO cells (Figures 3C and 3D). These proteomics data are remarkably consistent with the results of our U^{13}C-palmitate tracing studies (Figure 2B). We next performed RNA sequencing (RNA-seq) on DKO and TKO cells under the identical experimental conditions and again observed downregulation of the majority of FAO-related transcripts upon *Mcl-1* deletion in regular and low-glucose media (Figures 4A and 4B). To determine whether *Mcl-1* deletion selectively affects FAO or downregulates mitochondrial metabolism in general, we examined changes in transcript levels of 79 oxidative phosphorylation (OXPHOS) and 23 TCA cycle genes. Few if any changes were observed in these gene sets when comparing DKO and TKO cells in regular medium (Figures 4C and 4D), consistent with *Mcl-1* deletion exerting a selective effect on the FAO pathway.

Analogous disruption of FAO upon *Mcl-1* deletion in the presence of BAX and BAK

To determine whether our observations in DKO and TKO B-ALL cells extend to a cellular context in which deletion of *Mcl-1* is rescued by a mechanism other than co-deletion of *Bax* and *Bak*, we turned to p185$^+$*Arf*$^{-/-}$ B-ALL cells in which human *BCL-2* is overexpressed (p185$^+$*Arf*$^{-/-}$*Mcl-1*$^{-/-}$*hBCL-2*^{OE}) to enable cell survival upon *Mcl-1* deletion (Koss et al., 2013; Figure S3A). Although the MCL-1-dependent parental B-ALL cells are exquisitely sensitive to the selective MCL-1 inhibitor S63845 (Kotschy et al., 2016) but remain fully viable upon exposure to the selective BCL-2 inhibitor ABT-199 (Souers et al., 2013), the *Mcl-1*-deleted *BCL-2*-overexpressing cells demonstrate the opposite susceptibility profile (Figures S3B and S3C). In this system, metabolite tracing studies using ^{13}C-palmitate again revealed that *Mcl-1* deletion lowered the baseline percentage of M+2 citrate and blunted the response to the low-glucose condition (Figure S3D), confirming the adverse effect of *Mcl-1* deletion on FAO regardless of the presence of BAX and BAK. These data predict that, in the presence of BAX and BAK, pharmacological blockade of FAO should render the MCL-1-dependent parental cells more vulnerable to cell death than the BCL-2-dependent cells. We find that treatment with the FAO inhibitor ranolazine (Fragasso et al., 2007; German et al., 2016; Samudio et al., 2010), which targets 3-ketoacyl CoA thiolase (3-KAT), the fourth and final enzyme of the FAO cascade, dose-responsively impairs cell viability of the MCL-1-dependent cells with a comparatively minimal effect on the BCL-2-dependent cells over the 0–500 μM dosing range (Figure S3E).

We next sought to determine whether the observed impairment of FAO upon *Mcl-1* deletion could be rescued upon re-expression of *MCL-1*. For this experiment, we used p185$^+$*Arf*$^{-/-}$

B-ALL cells in which human *MCL-1* is overexpressed (p185$^+$*Arf*$^{-/-}$*Mcl-1*$^{-/-}$*hMCL-1*^{OE}) to enable cell survival upon *Mcl-1* deletion (Koss et al., 2013; Figure S3A). We observe that exogenous *MCL-1* expression phenocopies the exquisite sensitivity of the cells to S63845 and renders them resistant to ABT-199, rescuing anti-apoptotic activity (Figures S3B and S3C). In contrast, exogenous expression of *MCL-1* does not restore the FAO pathway (Figures S3D and S3E), suggesting that the mechanism of metabolic regulation by MCL-1 is distinct from that of apoptotic regulation, which relies on a direct interaction between the BH3-binding pocket of MCL-1 and the α-helical BH3 domain of pro-apoptotic BCL-2 family proteins. To verify this finding, we also reconstituted TKO cells with *MCL-1* (Figure S4A) and likewise observed no FAO rescue (Figure S4B). These data indicate that MCL-1 regulation of FAO may depend on expression from the endogenous *Mcl-1* genetic locus and sensing, feedback, or other circuitry embedded therein.

Finally, to determine whether our observations in the p185$^+$*Arf*$^{-/-}$ B-ALL cells extend to a completely distinct physiologic context, we analyzed transcriptomics data from wild-type versus *Mcl-1*$^{-/-}$ murine liver (*Bax* and *Bak* present). *Mcl-1*-deleted livers showed downregulation of the FAO gene set, with pathway analysis highlighting reductions in a series of defined FAO and peroxisome proliferator-activated receptor (PPAR) signaling networks (Figures 4E and 4F). The proteomics and transcriptomics data from the p185$^+$*Arf*$^{-/-}$ B-ALL cells (Figures 3C, 3D, 4A, and 4B) and murine livers (Figures 4E and 4F) demonstrate that, in the absence of MCL-1, the entire FAO program is blunted, pointing to a programmatic role of MCL-1 in regulating FAO.

Therapeutic implications of MCL-1 regulation of FAO in cancer

To validate our findings across human cancers and examine the potential therapeutic applications, we analyzed a dataset of metabolite levels in 928 cell lines that represent more than 20 cancer types in the Cancer Cell Line Encyclopedia (CCLE) (Li et al., 2019). Strikingly, a series of fatty acylcarnitines, the precursor substrates for FAO, ranked among the most negatively correlated metabolites with *MCL-1* expression (Figure 5A). Palmitoylcarnitine, a long-chain acylcarnitine, was the single most negatively correlated metabolite, particularly in hematologic, colon, ovarian, and pancreatic cancers (Figure 5B). Accumulation of fatty acylcarnitines *in vivo* typically indicates a block in FAO, as observed in inborn errors of fatty acid metabolism (Wanders et al., 1999). Conversely, the cancer cell findings suggest a link between elevated *MCL-1* expression and consumption of fatty acylcarnitines. Because the most striking inverse correlation between MCL-1 and palmitoylcarnitine levels occurred in hematologic malignancies, we interrogated comparative gene expression data from AML samples from affected individuals and normal bone marrow. We observed relative upregulation of *MCL-1* and FAO genes, including *CD36* and *CPT1A*, in addition to master transcriptional regulators of lipid metabolism, such as *PPARα*, *PPARγ*, and *PPARγ* coactivator 1α (*PGC1α*) Figure 5C). Other isoforms of these genes, including *PPARβ/δ* and *PGC1β*, as well as estrogen-related receptors (*ERRα*, *ERRβ*, and *ERRγ*), which constitute an additional transcription factor family capable of modulating FAO, were unchanged or downregulated in tumor samples (Figure 5D). Given the programmatic effects observed upon *Mcl-1* deletion in cancer cells and liver (Figures

3, 4, 5A, and 5B), the correlation in human AML between MCL-1 and PPARα, a key transcriptional regulator of FAO, is particularly intriguing (Figure 5C).

To examine whether the link between MCL-1 and FAO dependencies can be exploited for therapeutic benefit in cancer, we first validated a series of hematologic cancer cells as susceptible or resistant to the selective MCL-1 inhibitor S63845. Although S63845 dose-responsively impaired the viability of H929, MV4;11, OCI-AML2, 697, and OCI-AML3 cells, little to no effect was observed in U937, KCL-22, or K562 cells (Figure 6A). K-means clustering analysis based on an FAO gene set partitioned the cells into the same distinct clusters, indicating a correlation between MCL-1 dependency and FAO gene expression (Figure 6B). These data suggest that MCL-1-dependent hematologic cancer cells may be especially susceptible to pharmacological inhibition of FAO but relatively resistant to glucose withdrawal. To test this hypothesis, we subjected the panel of hematologic cancer cells to ranolazine and observed that the S63845-sensitive cells were distinctly susceptible, whereas the S63845-resistant lines were also resistant to ranolazine, even at 500 μM dosing (Figure 6C). Next, we selected the H929 and K562 cell lines, which, respectively, exhibited the most and least susceptibility to pharmacological MCL-1 inhibition by S63845, to evaluate the effect of glucose reduction on cell survival and proliferation. H929 and K562 cells were cultured in regular or low-glucose medium, and cell count was monitored over a 96-h period. Although proliferation of H929 cells was unaffected by withholding glucose, proliferation of K562 cells was markedly suppressed (Figures 6D and 6E). Viability studies showed that K562 cells, which were resistant to ranolazine when cultured in regular medium, became notably susceptible to ranolazine in low-glucose medium (Figure 6F). In contrast, H929 cells showed a comparatively modest decrement in viability because these cells were already sensitive to ranolazine in the presence of glucose (Figure 6F). These data suggest that K562 cells undergo a shift toward FAO upon glucose reduction for proliferation and survival, whereas H929 cells are driven by FAO at baseline. Metabolite tracing using ^{13}C-palmitate demonstrated an increased percentage of M+2 citrate in H929 cells compared with K562 cells in regular medium, consistent with heightened baseline utilization of palmitate and FAO in the MCL-1-dependent hematologic cancer cell line (Figure S5). When cultured in low-glucose medium, H929 and K562 cells, both of which express *MCL-1*, showed markedly increased palmitate utilization (Figure S5), explaining why H929 cells become even more sensitive to ranolazine upon glucose deprivation and why K562 cells transform from being ranolazine resistant to strikingly ranolazine sensitive (Figure 6F).

Having demonstrated that inhibiting the final enzymatic step of the FAO pathway renders MCL-1-dependent hematologic cancer cells vulnerable to cell death, we next tested blockade of FAO at one of the most apical steps of the pathway by targeting PPARα. Gene knockdown (Figure 6G) or treatment with the PPARα inhibitor GW6471 (Abu Aboud et al., 2013; Xu et al., 2002; Figure 6H) is selectively toxic to the MCL-1-dependent H929 cells. Glucose deprivation sensitized the MCL-1-independent K562 cells to PPARα inhibition (Figure 6H), paralleling the ranolazine results (Figure 6F) and indicating that a shift toward increased FAO utilization and dependency likely underlies this sensitization. Finally, the combination of GW6471 and the MCL-1 inhibitor S63845 was selectively cytotoxic in H929 cells (Figures 6I and S6). These results reveal a critical role of PPARα in the context of

MCL-1 dependency and demonstrate the potential therapeutic benefit of disrupting FAO in MCL-1-dependent cancer cells alone or in combination with blocking the anti-apoptotic functionality of MCL-1.

DISCUSSION

The level, spectrum, and occupancy of anti-apoptotic proteins expressed in cancer cells dictate the extent of apoptotic blockade and, thus, the response to standard chemotherapy and to inhibitors that target BCL-2 family proteins (Ni Chonghaile et al., 2011). MCL-1 is the most pervasively expressed anti-apoptotic protein in cancer and has been implicated in chemoresistance and relapsed disease (Akgul, 2009; Beroukhim et al., 2010). Although BCL-2 was the first BCL-2 family member to be successfully drugged (Souers et al., 2013), MCL-1 is next in line, with multiple selective inhibitors currently undergoing clinical testing in human cancers (Wang et al., 2021). Several MCL-1 inhibitor trials were halted because of concerning side effects, such as cardiotoxicity, which was first observed upon conditional deletion of *Mcl-1* in mice (Wang et al., 2013). Genetic deletion of *Mcl-1*, whether global or conditional, causes striking phenotypes that, by definition, are not compensated for by anti-apoptotic homologs (Opferman et al., 2003, 2005; Perciavalle et al., 2012; Rinkenberger et al., 2000; Wang et al., 2013). These findings suggest that MCL-1 has additional, non-apoptotic roles that may (1) underlie cancer pathogenesis, chemoresistance, and the toxicity of current MCL-1 inhibitors and (2) inform the development of novel therapeutic strategies.

A growing body of studies highlights the critical role of FAO in fueling human cancers (Carracedo et al., 2013; Ma et al., 2018). Metabolic reprogramming of cancer cells to rely on fatty acids is a formidable chemoresistance mechanism, and pharmacological inhibition of FAO can restore apoptosis (Caro et al., 2012; German et al., 2016; Pascual et al., 2017; Samudio et al., 2010). Fatty acid metabolism has been shown recently to account for resistance to combined venetoclax and azacytidine treatment in AML stem cells, and small-molecule inhibition of MCL-1 decreased fatty acid metabolism (Stevens et al., 2020). The mechanism of action has been proposed to involve, at least in part, the MCL-1^{Matrix}/VLCAD interaction (Escudero et al., 2018), with knockdown of *Acadvl* resensitizing primary AML specimens to the venetoclax/azacytidine combination (Stevens et al., 2020). In another AML study, gene knockdown or pharmacological inhibition of MCL-1 decreased OCR and ATP production in addition to adversely affecting the TCA cycle, glycolysis, and the pentose phosphate pathway (Carter et al., 2020). Because inhibiting MCL-1 with small molecules that target its BH3-binding groove effectively triggers mitochondrial apoptosis, particularly in combination with venetoclax (Hormi et al., 2020), delineating a separable role for MCL-1 in metabolic regulation is confounded. To date, data that link MCL-1 to metabolism include the requirement of MCL-1^{Matrix} for normal mitochondrial respiration, ATP production, and oligomeric ATP synthase assembly (Anilkumar et al., 2020; Perciavalle et al., 2012). This discrete isoform of MCL-1 has been shown to modulate long-chain FAO through direct MCL-1 BH3 interaction with VLCAD (Escudero et al., 2018). Despite mounting evidence that links MCL-1, FAO, cancer progression, and chemoresistance, whether and how MCL-1 exerts a mechanistic function that is wholly distinct from anti-apoptotic activity remained unknown.

Here we studied the influence of *Mcl-1* deletion in the context of BAX/BAK deficiency to distinguish a non-canonical role of MCL-1 in regulating FAO in leukemia cells. In the absence of mitochondrial apoptosis, we observed that MCL-1 dictates a fuel dependency on lipids such that, upon *Mcl-1* deletion, leukemia cells cannot survive glucose deprivation. Alternative fuels that can provide sources of acetyl-CoA for the TCA cycle rescued this non-apoptotic cell death, suggesting that a specific energetic/metabolic defect underlies the inability of cells lacking MCL-1 to withstand glucose deprivation. We find that these data are relevant to therapeutic intervention in that MCL-1-dependent hematologic cancer cells are selectively sensitive to FAO inhibition, and MCL-1-independent cancer cells become sensitized to FAO inhibition upon glucose deprivation. Metabolic studies documented that MCL-1 is required to specifically maintain fatty acid levels and increased FAO at baseline and in response to glucose deprivation. Proteomics and transcriptomics analyses demonstrated that MCL-1 correspondingly sustains the transcription of FAO genes and expression of FAO proteins at a programmatic level. This global effect of MCL-1 on FAO gene expression was corroborated by analyses of wild-type versus *Mcl-1$^{-/-}$* livers. The remarkable extent of MCL-1's effect on the FAO pathway mirrors that of PPARα itself, with knockdown or molecular inhibition of PPARα selectively detrimental to MCL-1-dependent hematologic cancer cells.

The direct correlation we observed in human AML datasets between *MCL-1* and FAO gene expression and the striking inverse correlation between *MCL-1* expression and fatty acylcarnitine levels across more than 900 human cancers suggest that MCL-1's role in FAO regulation includes but extends beyond the MCL-1^{Matrix} interaction with VLCAD. What we uncovered here, by examining the influence of *Mcl-1* deletion in the context of MCL-1 dependency and in the absence of mitochondrial apoptosis, is unexpected and striking: in addition to its cardinal role in suppressing apoptosis, MCL-1 appears to function as a master regulator of the entire FAO program.

Limitations of the study

A major challenge in elucidating non-canonical roles of BCL-2 family proteins is their established functionalities in regulating the life-death decision of the cell in response to stress. Thus, is the death response upon genetic deletion of *Mcl-1* in an experimental context such as glucose deprivation due to loss of anti-apoptotic function, a defect in a distinct MCL-1-regulated pathway, or some combination? Here, to examine a role of MCL-1 in regulating the FAO pathway, we used genetically defined murine leukemia cells that are exquisitely dependent on MCL-1 and would otherwise die in the absence of MCL-1 if not for co-deletion of *Bax* and *Bak* or overexpression of another anti-apoptotic gene such as *BCL-2*. Although this system represents a genetically engineered context, the phenotypic consequences for metabolism upon *Mcl-1* deletion are the same whether cell survival is maintained by deletion of *Bax/Bak* or overexpression of *BCL-2*, which is reassuring in that potential collaborating roles of *Bax/Bak* deletion or *BCL-2* overexpression are essentially ruled out. To test for rescue of the phenotype upon re-expression of *MCL-1*, we overexpressed the human form, which runs at a higher molecular weight, prior to deletion of the murine isoform to definitively select for cells expressing human rather than murine *Mcl-1*. Although this experimental strategy successfully rescues anti-apoptotic functionality,

we did not observe metabolic rescue. These data suggest that MCL-1 regulation of FAO is distinct from that of apoptosis and may require expression from the endogenous locus to maintain the signaling circuit, which appears to involve master regulation of an FAO transcriptional program. However, we cannot exclude, from the current experiments, that the human sequence is sufficiently distinct from that of the murine isoform to underlie the lack of rescue. To validate our findings, we turned to a series of orthogonal inquires, evaluating correlations between MCL-1 and FAO in wild-type versus murine liver, human AML datasets, and MCL-1-dependent versus independent human hematologic cancer cells. In each case, the same theme emerged: deletion of *Mcl-1* results in a downregulated FAO pathway, whereas upregulated MCL-1 correlates with a reliance on FAO and, thus, a striking vulnerability to FAO inhibition.

Our finding that *Mcl-1* expression underlies cancer dependency on FAO through a mechanism independent from apoptotic regulation raises a series of follow-up questions. (1) What is the explicit mechanism by which MCL-1 regulates FAO? (2) Does the MCL-1 control point lie upstream or downstream of PPARα? (3) Can targeting the canonical BH3-binding pocket of MCL-1 influence its metabolic role, or is another protein interaction surface involved? (4) Do the toxicities associated with MCL-1 inhibitors in affected individuals derive from inducing apoptosis, disrupting FAO, or both? Future studies that address these questions will continue to expand our understanding of the uniquely complex biology of MCL-1 and facilitate the development of safe and effective MCL-1-targeted treatments. In the interim, however, based on comprehensive and multidisciplinary analyses, we provide a specific and compelling rationale for targeting FAO in MCL-1-dependent cancers to combat relapsed and refractory disease.

STAR★METHODS

RESOURCE AVAILABILITY

Lead contact—Further information and requests for resources and reagents should be directed to and will be fulfilled or facilitated by the lead contact Loren Walensky (loren_walensky@dfci.harvard.edu).

Materials availability—Plasmids and cell lines generated in this study are available upon request to the lead contact. The B-ALL cell lines are available upon request to co-author Joseph Opferman (joseph.opferman@stjude.org).

Data and code availability

- The data supporting the findings of this study are available within the article and its supplemental information. Metabolomics, proteomics, and RNA-seq datasets were submitted to the following depositories, respectively: MetaboLights: MTBLS4225, ProteomeXchange via PRIDE: PXD031364, and NCBI GEO: GSE196136.

- This paper does not report original code.

- Any additional information required to reanalyze the data reported in this paper
  is available from the lead contact upon request.

EXPERIMENTAL MODEL AND SUBJECT DETAILS

Murine parental, $Bax^{-/-}Bak^{-/-}$ (DKO), $Bax^{-/-}Bak^{-/-}Mcl-1^{-/-}$ (TKO), $Bax^{-/-}Bak^{-/-}Mcl-1^{-/-}hMCL-1$ (TKO + MCL-1), $Mcl-1^{-/-}hBCL-2^{OE}$ (BCL-2^{OE}), and $Mcl-1^{-/-}hMCL-1^{OE}$ (MCL-1^{OE}) p185$^+$ $Arf^{-/-}$ B-ALL cell lines were provided by Joseph Opferman and were cultured in Roswell Park Memorial Institute (RPMI) 1640 (Thermo Fisher Scientific, catalog #21870-076) supplemented with 10% (v/v) fetal bovine serum, 100 U/mL penicillin and streptomycin, 2 mM glutamine, 10 mM HEPES, 100 μM Minimum Essential Medium (MEM) non-essential amino acids, and 55 μM 2-mercaptoethanol. The parental, DKO, TKO, BCL-2^{OE}, and MCL-1^{OE} B-ALL cell lines were generated previously (Koss et al., 2013, 2016), and the TKO+MCL-1 B-ALL cell line was generated by transducing the TKO cells with MSCV-puro-hMCL-1 and selecting with 1 μg/mL puromycin. Human hematologic cancer cell lines (H929, MV4;11, OCI-AML2, 697, OCI-AML3, U937, KCL-22, K562) were cultured in RPMI 1640 supplemented with 10% (v/v) fetal bovine serum, 100 U/mL penicillin and streptomycin, and 2 mM glutamine. All cell lines were maintained at 37°C with 5% CO_2. Cells were verified as mycoplasma negative using the MycoAlert mycoplasma detection kit (Lonza Biologics, catalog #LT07-218) prior to experimental studies.

METHOD DETAILS

Western blot analysis—Parental, DKO, TKO, TKO+MCL-1, BCL-2^{OE}, and MCL-1^{OE} B-ALL cells were lysed in NP-40 lysis buffer (50 mM Tris, pH 7.4, 150 mM NaCl, 0.5% [v/v] NP-40, complete protease inhibitor tablet [Roche, catalog #05056489001]). Cell debris was pelleted at 13,000 rpm for 10 minutes at 4°C, and protein concentration of the supernatant was quantified using the BCA Protein Assay Kit (Thermo Fisher Scientific, catalog #23225). Lysates (30 μg) were subjected to gel electrophoresis and western blotting using the indicated antibodies at 1:1000 in 5% (w/v) BSA in TBS-T: MCL-1 (Rockland Immunochemicals, catalog #600-401-394, RRID AB_2266446), BAX (Cell Signaling Technology, catalog #14796S, RRID AB_2716251), BAK (Cell Signaling Technology, catalog #12105S, RRID AB_2716685), BCL-2 (Santa Cruz Biotechnology, catalog #sc-509 HRP, RRID AB_626733), and actin (Cell Signaling Technology, catalog # 5125S, RRID AB_1903890).

Cell viability assays—For glucose deprivation of B-ALL cells, 200,000 cells/well were plated in 12-well plates in regular or low glucose media for the indicated incubation times. Low glucose media consisted of RPMI lacking glucose (Thermo Fisher Scientific, catalog #11879-020) supplemented as described above for B-ALL cell lines. Regular and low glucose media contained 2.59 g/L and 0.05 g/L glucose, respectively, as determined by glucometer measurements. Cell survival was measured by staining cells with 1 μg/mL propidium iodide (Thermo Fisher Scientific) in 1x PBS and performing flow cytometry on a BD LSRFortessa. Metabolic rescue experiments were performed similarly, except with the addition of vehicle (H_2O), sodium pyruvate, or sodium acetate at a final concentration of 10 mM to the low glucose media for 72 hours. For S63845 and ABT-199 treatments,

5,000 cells/well were plated in 96-well plates and incubated with vehicle (0.01% DMSO for S63845 and 0.001% DMSO for ABT-199) or drug (Selleck Chemicals) at the indicated doses for 48 hours. Viability was measured by CellTiter-Glo (Promega) following the manufacturer's instructions and plotted as percent viable relative to vehicle. For ranolazine treatments of B-ALL cells, 200,000 cells/well were plated in 12-well plates and incubated with vehicle (H_2O) or drug (Selleck Chemicals) at the indicated doses for 48 hours. Survival was measured by propidium iodide staining and flow cytometry. For ranolazine and GW6471 treatments of hematologic cancer cells, 100,000 cells/well were plated in 12-well plates and treated with vehicle (H_2O for ranolazine or 0.02% DMSO for GW6471) or drug (Selleck Chemicals) at the indicated doses. For ranolazine, fresh drug was added after 48 hours. Survival was measured 96 hours after the initial treatment by propidium iodide staining and flow cytometry. Ranolazine or GW6471 treatment in combination with glucose deprivation was performed similarly but with cells plated in regular or low glucose media, which consisted of RPMI lacking glucose supplementation, as described above for hematologic cancer cell lines. S63845 and GW6471 combination treatments were performed similarly with cells treated with vehicle (0.01% DMSO) or the indicated doses of drug(s). For gene knockdown studies, H929 and K562 cells were plated at 200,000 cells/mL in 24-well plates in RPMI supplemented with 1% FBS, 100 U/mL penicillin and streptomycin, and 2 mM glutamine, and treated with vehicle (1x siRNA buffer diluted from 5x siRNA buffer [Horizon Discovery, catalog #B-002000-UB-100] using RNase-free H_2O [Horizon Discovery, catalog #B-003000-WB-100]), 1 mM Accell non-targeting control siRNA pool (Horizon Discovery, catalog #D-001910-10-05), or 1 μM Accell human PPARα siRNA pool (Horizon Discovery, catalog #E-003434-00-0005) for 96 hours, followed by propidium iodide staining and flow cytometry. Percent cell survival was calculated and plotted relative to vehicle.

Electron microscopy—DKO and TKO B-ALL cells were plated at 200,000 cells/mL in regular or low glucose media, as defined above. After 48 hours, 3 million cells for each sample were centrifuged at 1,000 rpm for 5 minutes and resuspended in 250 μL media. Fixative was prepared by diluting glutaraldehyde (25%) to 5% in a 0.1 M sodium cacodylate pH 7.4 buffer containing 2.5% formaldehyde and 0.06% picric acid. The fixative was added at a ratio of 1:1 (250 μL) to the cells. After a 5-minute incubation at room temperature, samples were centrifuged and processed at the Electron Microscopy Facility of Harvard Medical School. The samples were embedded in Epon resin, cut into ultrathin sections, and imaged by transmission electron microscopy (TEM) using a JEOL 1200EX microscope equipped with an AMT 2k CCD camera.

Seahorse analysis—Oxygen consumption rate (OCR) was measured in real time using the XF24 extracellular flux analyzer instrument and the Seahorse Wave software (Agilent Technologies) as described previously (Caro et al., 2012). Briefly, DKO and TKO B-ALL cells were plated on XF24 V7 plates coated with 22.4 μg/mL Cell-Tak (Corning, catalog #354240) at 300,000 cells/well in 500 μL of sodium bicarbonate-free RPMI media (without glucose, glutamine, and sodium pyruvate) alone or supplemented with 200 μM palmitate and 500 μM carnitine. OCR measurements were taken after 1 hour.

Metabolite tracing studies—Cells were plated at 500,000 cells/mL in 6-well plates in the indicated media. After 24 hours, cells were labeled with 50 μM U^{13}C-palmitate, 200 μM 1 ^{13}C-hexanoate, or 10 mM U^{13}C-glucose for 2 hours. Metabolites were extracted as previously described (Faubert et al., 2013). Briefly, cells were pelleted and washed twice with ice-cold 0.9% sodium chloride, followed by metabolite extraction using ice-cold 80% methanol. The extracts were sonicated on an ice bath (Bioruptor, diagenode) at high intensity with a 30 second on/off cycle for 10 minutes. Subsequently, the samples were centrifuged at 16,400 rpm for 20 minutes at 4°C, and the supernatants dried overnight using a vacuum concentrator. On the following day, two step derivatizations were carried out as follows: samples were incubated with 30 μL of MOX solution from the stock of 120 mM methoxyamine (Sigma-Aldrich, catalog #226904) dissolved in pyridine (Sigma-Aldrich, catalog #270970) at 37°C for 30 minutes, followed by silylation with 70 μL of *N-tert-*Butyldimethylsilyl-*N*-methyltrifluoroacetamide (MTBSTFA, Sigma-Aldrich, catalog #394882) at 60°C for 1 hour. Metabolites were analyzed using GC-MS as described previously (Faubert et al., 2014; Fu et al., 2020; Mamer et al., 2013; McGuirk et al., 2013). Briefly, samples were run on an Agilent 7890B gas chromatograph with a DB-5MS+DG capillary column (30 m plus 10 m Duraguard® by Agilent Technologies) coupled to a 5977B mass selective detector (Fu et al., 2020). Data were collected in full scan mode (1–600 m/z). All the metabolites measured were previously validated standards with mass spectra and retention times (Mamer et al., 2013). Peak area integration was carried out using MassHunter Quantitative Analysis (Agilent Technologies). ^{13}C enrichment was calculated using previously developed algorithms, including natural isotope enrichment correction and mass isotope distributions (MIDs) (Fu et al., 2020; McGuirk et al., 2013; Nanchen et al., 2007).

Measurement of free fatty acid levels—DKO and TKO B-ALL cells were plated at 500,000 cells/mL in regular or low glucose media. After 24 hours, 3 million cells per sample were centrifuged at 1,000 rpm for 5 minutes and washed once with 1x PBS. Supernatants were removed and cell pellets were shipped on dry ice to the Metabolomics Facility at Washington University (P30 DK020579) for analysis. Cell suspensions (1×10^7 cells/mL) were prepared by vortexing cell pellets with H_2O. Protein precipitation was performed to extract free fatty acids (FFA) from 50 μL of cell suspension. The d4-FFA (16:0) was used as an internal standard, which was added to the samples before extraction. Analysis of FFAs was performed in positive MRM mode on a 4000QTRAP mass spectrometer coupled to a Shimadzu 20A HPLC system. Data processing was conducted with Analyst 1.6.3. Quality control (QC) samples were prepared by pooling aliquots of the samples and were used to monitor instrument performance. The QC samples were injected between every five experimental samples. Only the lipid species with coefficient of variance less than 15% in QC injections were reported. The relative quantification of lipids was provided as the peak area ratios of the analytes to the corresponding internal standards.

Untargeted metabolomics—DKO and TKO B-ALL cells were plated at 500,000 cells/mL in regular media in 6-well plates. After 24 hours, cells were centrifuged at 1,000 rpm for 5 minutes and washed with 3 mL freshly prepared 75 mM ammonium carbonate in HPLC grade water (pH adjusted to 7.4 with HPLC grade formic acid). Cells were

centrifuged, supernatants were removed, and 700 μL of 70% ethanol pre-heated to 70°C was added, followed by a 3-minute incubation. The extracts were transferred to microcentrifuge tubes on dry ice and then centrifuged at 14,000 rpm for 10 minutes at 4°C. Extract supernatants were transferred to new microcentrifuge tubes and subjected to high-throughput non-targeted metabolomics. These analyses were performed using the services of General Metabolics, LLC on a platform consisting of an Agilent 1260 Infinity II LC pump coupled to a Gerstel MPS autosampler (CTC Analytics) and an Agilent 6550 Series Quadrupole TOF mass spectrometer with Dual AJS ESI source operating in negative ion mode as described previously (Fuhrer et al., 2011). All steps of mass spectrometry data processing and analysis were performed with MATLAB using functions embedded in the Bioinformatics, Statistics, Database, and Parallel Computing toolboxes as described previously (Fuhrer et al., 2011).

Global proteomics

Sample preparation: DKO and TKO B-ALL cells were plated at 500,000 cells/mL in 6-well plates in regular or low glucose media, as defined above. After 24 hours, cells were harvested and lysed in CHAPS buffer. The resulting lysates were quantified by the BCA Protein Assay Kit (Thermo Fisher Scientific, catalog #23225) and subsequently reduced, alkylated, and subjected to chloroform/methanol precipitation (Navarrete-Perea et al., 2018). Protein precipitates were then resuspended in 100 μL of 200 mM EPPS buffer, pH 8.5 before proteolytic digestion by LysC (overnight) and trypsin (6 hours). Tryptic peptides were subsequently processed in highly parallel fashion using isobaric tagging (TMTpro16-plex) (Li et al., 2020), followed by 1:1 mixing across all channels. Samples were then desalted using a 100 mg Sep-Pak solid-phase extraction column. We fractionated the pooled, labeled peptide sample using BPRP HPLC (Wang et al., 2011). We used an Agilent 1200 pump equipped with a degasser and a detector set at 220 and 280 nm wavelength. Peptides were subjected to a 50-min linear gradient from 5% to 35% acetonitrile in 10 mM ammonium bicarbonate pH 8 at a flow rate of 0.6 mL/min over an Agilent 300Extend C18 column (3.5 μm particles, 4.6 mm ID and 220 mm in length). The peptide mixture was fractionated into a total of 96 fractions, which were consolidated into 24 super-fractions (Paulo et al., 2016). Samples were subsequently acidified with 1% formic acid and vacuum centrifuged to near dryness. Each consolidated fraction was desalted via StageTip, dried again via vacuum centrifugation, and reconstituted in 5% acetonitrile, 5% formic acid for LC-MS/MS processing.

Liquid chromatography and tandem mass spectrometry: Mass spectrometric data were collected on an Orbitrap Fusion Lumos mass spectrometer with the FAIMS Pro interface (Thermo Fisher Scientific) coupled to a Proxeon EASY-nLC 1200 liquid chromatograph (LC) (Thermo Fisher Scientific). Peptides were separated on a 100 μm inner diameter microcapillary column packed with ~35 cm of Accucore150 resin (2.6 μm, 150 Å, Thermo Fisher Scientific). For each analysis, we loaded 1 to 2 μg of peptide onto the column and fractionated over a 90 min gradient of 4 to 27% acetonitrile in 0.125% formic acid at a flow rate of ~450 nL/min. Mass spectrometric data were collected using an RTS-MS3 (Schweppe et al., 2020) method with High-field asymmetric-waveform ion mobility spectrometry (FAIMS). The scan sequence began with an MS1 spectrum (Orbitrap analysis; resolution, 60,000; mass range, 400–1600 Th; automatic gain control (AGC) target 100%; maximum

injection time, auto). Precursors were then selected for MS2/MS3 analysis (Ting et al., 2011). MS2 analysis consisted of collision-induced dissociation (CID) with quadrupole ion trap analysis, using the following parameters: scan speed, turbo; AGC target, 100%; NCE, 35; q-value, 0.25; maximum injection time, 35 ms; and isolation window, 0.5 Th. MS3 precursors were fragmented by HCD and analyzed using the Orbitrap with the following parameters: resolution, 50,000; NCE, 55; AGC, 200,000; maximum injection time, 250 ms; maximum synchronous precursor selection (SPS) ions, 10; and isolation window, 1.2 Th. Data were collected with the "close-out" parameter set to 2.

Data analysis: Mass spectra were processed using a Comet-based software pipeline (Eng et al., 2013, 2015). Database searching included all entries from the mouse UniProt database (March 20, 2020). This database was concatenated with one composed of all protein sequences in the reversed order. Searches were performed using a 50-ppm precursor ion tolerance and the product ion tolerance was set to 0.9 Da for SPS-MS3. Enzyme specificity was assigned as trypsin. TMTpro labels on lysine residues and peptide N termini (+304.207) and carbamidomethylation of cysteine residues (+57.021 Da) were set as static modifications, while oxidation of methionine residues (+15.995 Da) was set as a variable modification. Peptide-spectrum matches (PSMs) were adjusted to a 1% false discovery rate (FDR) (Elias and Gygi, 2007, 2010). PSM filtering was performed using a linear discriminant analysis, as described previously (Huttlin et al., 2010), while considering the following parameters: XCorr, peptide length, Cn, charge state, missed cleavages, and mass accuracy of the precursor. For TMT-based reporter ion quantitation, we extracted the signal-to-noise (S:N) ratio for each TMT channel and found the closest matching centroid to the expected mass of the TMT reporter ion. PSMs were identified, quantified, and collapsed to a 1% peptide FDR and then collapsed further to a final protein-level FDR of 1%. Peptide intensities were quantified by summing reporter ion counts across all matching PSMs so as to give greater weight to more intense ions (McAlister et al., 2012, 2014).

RNA-seq—DKO and TKO B-ALL cells were plated at 500,000 cells/mL in regular or low glucose media, as defined above. After 24 hours, 10 million cells per sample were centrifuged and washed once with 1x PBS. Supernatants were removed and total RNA was extracted using the Qiagen RNeasy Mini Kit following the manufacturer's instructions. RNA samples were submitted to the Molecular Biology Core Facility at the Dana-Farber Cancer Institute for library construction and sequencing. Libraries were prepared using the Roche Kapa mRNA HyperPrep strand specific sample preparation kit from 200 ng of purified total RNA according to the manufacturer's protocol on a Beckman Coulter Biomek i7. The finished dsDNA libraries were quantified by Qubit fluorometer and Agilent TapeStation 4200. Uniquely dual indexed libraries were pooled in equimolar ratios and shallowly sequenced on an Illumina MiSeq to further evaluate library quantity and pool balance. The final pool was sequenced on an Illumina NovaSeq6000 targeting 40 million 100 bp read pairs per library. Sequenced reads were then aligned to the UCSC mm10 reference genome assembly and gene counts were quantified using STAR v2.7.3a (Dobin et al., 2013). Differential gene expression testing was performed by DESeq2 v1.22.1 (Love et al., 2014). RNA-seq analysis was performed using the VIPER snakemake pipeline (Cornwell et al., 2018).

Analysis of murine liver transcriptomic data—Differential gene expression analysis of a publicly available GEO dataset (GSE75730) comparing *Mcl-1* deleted murine livers (AlbCre$^+$*Mcl-1*$^{fl/fl}$) to wild-type controls (Boege et al., 2017) was performed using the NCBI online tool GEO2R (Barrett et al., 2013). Genes downregulated upon *Mcl-1* deletion were subjected to pathway enrichment analysis and queried against the WikiPathways Mouse (2019) database using the integrative web-based application Enrichr (Chen et al., 2013; Kuleshov et al., 2016).

Analysis of cancer metabolomic data—Gene expression data for *MCL-1* (Expression 19Q2 Public) and metabolite profiling data (Metabolomics 19Q2) (Li et al., 2019) for human cancer cell lines from 20 major cancer types in the Cancer Cell Line Encyclopedia (CCLE) were downloaded from the Dependency Map (DepMap) Portal (Broad Institute). For correlation analysis, the dataset was first filtered for polar metabolites, and Pearson correlation with *MCL-1* expression computed and plotted as a ranked list. For cancer type specific analysis, cancer cell lines were binned into quartiles based on *MCL-1* expression levels (High, Medium/High, Low/Medium, Low) and the mean $\log_{10}$ transformed intensity values for palmitoylcarnitine within each quartile were plotted.

Differential gene expression analysis—Gene expression datasets from human AML and bone marrow were analyzed using GEPIA2 (Tang et al., 2019) based on RNA-seq data from The Cancer Genome Atlas (TCGA) and the Genotype-Tissue Expression (GTEx) projects, respectively.

K-means clustering analysis—The panel of hematologic cancer cell lines (H929, MV4;11, OCI-AML2, 697, OCI-AML3, U937, KCL-22, K562) was subjected to unsupervised clustering (k-means, k = 2) based on expression levels of an FAO gene set.

Cell proliferation assays—H929 and K562 cells were plated at 400,000 cells/mL in regular or low glucose media, as defined above. Cell counts were determined by trypan blue staining at baseline and 24-hour intervals through 96 hours.

QUANTIFICATION AND STATISTICAL ANALYSIS

Replicate information for each experiment can be found in the figure legends. An unpaired two-tailed Student's t test using GraphPad Prism software was used to determine significant difference between two variables. Statistical significance for RNA-seq data was calculated using the Wald test, with correction for multiple hypothesis testing using the Benjamini-Hochberg method. Statistical significance for untargeted metabolomics was calculated using the z-test, with correction for multiple hypothesis testing by the Benjamini-Hochberg method.

Supplementary Material

Refer to Web version on PubMed Central for supplementary material.

ACKNOWLEDGMENTS

REFERENCES

Abu Aboud O, Wettersten HI, and Weiss RH (2013). Inhibition of PPARalpha induces cell cycle arrest and apoptosis, and synergizes with glycolysis inhibition in kidney cancer cells. PLoS One 8, e71115. 10.1371/journal.pone.0071115. [PubMed: 23951092]

Akgul C (2009). Mcl-1 is a potential therapeutic target in multiple types of cancer. Cell. Mol. Life Sci 66, 1326–1336. 10.1007/s00018-008-8637-6. [PubMed: 19099185]

Anilkumar U, Khacho M, Cuillerier A, Harris R, Patten DA, Bilen M, Iqbal MA, Guo DY, Trudeau LE, Park DS, et al. (2020). MCL-1(Matrix) maintains neuronal survival by enhancing mitochondrial integrity and bioenergetic capacity under stress conditions. Cell Death Dis. 11, 321. 10.1038/s41419-020-2498-9. [PubMed: 32371858]

Barrett T, Wilhite SE, Ledoux P, Evangelista C, Kim IF, Tomashevsky M, Marshall KA, Phillippy KH, Sherman PM, Holko M, et al. (2013). NCBI GEO: archive for functional genomics data sets–update. Nucleic Acids Res. 41, D991–D995. 10.1093/nar/gks1193. [PubMed: 23193258]

Beroukhim R, Mermel CH, Porter D, Wei G, Raychaudhuri S, Donovan J, Barretina J, Boehm JS, Dobson J, Urashima M, et al. (2010). The landscape of somatic copy-number alteration across human cancers. Nature 463, 899–905. 10.1038/nature08822. [PubMed: 20164920]

Boege Y, Malehmir M, Healy ME, Bettermann K, Lorentzen A, Vucur M, Ahuja AK, Böhm F, Mertens JC, Shimizu Y, et al. (2017). A dual role of caspase-8 in triggering and sensing proliferation-associated DNA damage, a key determinant of liver cancer development. Cancer Cell 32, 342–359.e10. 10.1016/j.ccell.2017.08.010. [PubMed: 28898696]

Caro P, Kishan AU, Norberg E, Stanley IA, Chapuy B, Ficarro SB, Polak K, Tondera D, Gounarides J, Yin H, et al. (2012). Metabolic signatures uncover distinct targets in molecular subsets of diffuse large B cell lymphoma. Cancer Cell 22, 547–560. 10.1016/j.ccr.2012.08.014. [PubMed: 23079663]

Carracedo A, Cantley LC, and Pandolfi PP (2013). Cancer metabolism: fatty acid oxidation in the limelight. Nat. Rev. Cancer 13, 227–232. 10.1038/nrc3483. [PubMed: 23446547]

Carter BZ, Mak PY, Tao W, Warmoes M, Lorenzi PL, Mak D, Ruvolo V, Tan L, Cidado J, Drew L, et al. (2020). Targeting MCL-1 dysregulates cell metabolism and leukemia-stroma interactions and resensitizes acute myeloid leukemia to BCL-2 inhibition. Haematologica 107, 58–76. 10.3324/haematol.2020.260331.

Chen EY, Tan CM, Kou Y, Duan Q, Wang Z, Meirelles GV, Clark NR, and Ma'ayan A (2013). Enrichr: interactive and collaborative HTML5 gene list enrichment analysis tool. BMC Bioinf. 14, 128. 10.1186/1471-2105-14-128.

Cornwell M, Vangala M, Taing L, Herbert Z, Köster J, Li B, Sun H, Li T, Zhang J, Qiu X, et al. (2018). VIPER: visualization Pipeline for RNA-seq, a Snakemake workflow for efficient and complete RNA-seq analysis. BMC Bioinf. 19, 135. 10.1186/s12859-018-2139-9.

Czabotar PE, Lessene G, Strasser A, and Adams JM (2014). Control of apoptosis by the BCL-2 protein family: implications for physiology and therapy. Nat. Rev. Mol. Cell Biol 15, 49–63. 10.1038/nrm3722. [PubMed: 24355989]

Danial NN, Gramm CF, Scorrano L, Zhang CY, Krauss S, Ranger AM, Datta SR, Greenberg ME, Licklider LJ, Lowell BB, et al. (2003). BAD and glucokinase reside in a mitochondrial complex that integrates glycolysis and apoptosis. Nature 424, 952–956. 10.1038/nature01825. [PubMed: 12931191]

Danial NN, and Korsmeyer SJ (2004). Cell death: critical control points. Cell 116, 205–219. 10.1016/s0092-8674(04)00046-7. [PubMed: 14744432]

Dobin A, Davis CA, Schlesinger F, Drenkow J, Zaleski C, Jha S, Batut P, Chaisson M, and Gingeras TR (2013). STAR: ultrafast universal RNA-seq aligner. Bioinformatics 29, 15–21. 10.1093/bioinformatics/bts635. [PubMed: 23104886]

Elias JE, and Gygi SP (2007). Target-decoy search strategy for increased confidence in large-scale protein identifications by mass spectrometry. Nat. Methods 4, 207–214. 10.1038/nmeth1019. [PubMed: 17327847]

Elias JE, and Gygi SP (2010). Target-decoy search strategy for mass spectrometry-based proteomics. Methods Mol. Biol 604, 55–71. 10.1007/978-1-60761-444-9_5. [PubMed: 20013364]

Eng JK, Hoopmann MR, Jahan TA, Egertson JD, Noble WS, and MacCoss MJ (2015). A deeper look into Comet–implementation and features. J. Am. Soc. Mass Spectrom 26, 1865–1874. 10.1007/s13361-015-1179-x. [PubMed: 26115965]

Eng JK, Jahan TA, and Hoopmann MR (2013). Comet: an open-source MS/MS sequence database search tool. Proteomics 13, 22–24. 10.1002/pmic.201200439. [PubMed: 23148064]

Escudero S, Zaganjor E, Lee S, Mill CP, Morgan AM, Crawford EB, Chen J, Wales TE, Mourtada R, Luccarelli J, et al. (2018). Dynamic regulation of long-chain fatty acid oxidation by a noncanonical interaction between the MCL-1 BH3 helix and VLCAD. Mol. Cell 69, 729–743.e7. 10.1016/j.molcel.2018.02.005. [PubMed: 29499131]

Farrow SN, White JH, Martinou I, Raven T, Pun KT, Grinham CJ, Martinou JC, and Brown R (1995). Cloning of a bcl-2 homologue by interaction with adenovirus E1B 19K. Nature 374, 731–733. 10.1038/374731a0. [PubMed: 7715729]

Faubert B, Boily G, Izreig S, Griss T, Samborska B, Dong Z, Dupuy F, Chambers C, Fuerth BJ, Viollet B, et al. (2013). AMPK is a negative regulator of the Warburg effect and suppresses tumor growth in vivo. Cell Metab. 17, 113–124. 10.1016/j.cmet.2012.12.001. [PubMed: 23274086]

Faubert B, Vincent EE, Griss T, Samborska B, Izreig S, Svensson RU, Mamer OA, Avizonis D, Shackelford DB, Shaw RJ, et al. (2014). Loss of the tumor suppressor LKB1 promotes metabolic reprogramming of cancer cells via HIF-1alpha. Proc. Natl. Acad. Sci. USA 111, 2554–2559. 10.1073/pnas.1312570111. [PubMed: 24550282]

Fragasso G, Spoladore R, Cuko A, and Palloshi A (2007). Modulation of fatty acids oxidation in heart failure by selective pharmacological inhibition of 3-ketoacyl coenzyme-A thiolase. Curr. Clin. Pharmacol 2, 190–196. 10.2174/157488407781668776. [PubMed: 18690865]

Fu A, Alvarez-Perez JC, Avizonis D, Kin T, Ficarro SB, Choi DW, Karakose E, Badur MG, Evans L, Rosselot C, et al. (2020). Glucose-dependent partitioning of arginine to the urea cycle protects beta-cells from inflammation. Nat. Metab 2, 432–446. 10.1038/s42255-020-0199-4. [PubMed: 32694660]

Fuhrer T, Heer D, Begemann B, and Zamboni N (2011). High-throughput, accurate mass metabolome profiling of cellular extracts by flow injection-time-of-flight mass spectrometry. Anal. Chem 83, 7074–7080. 10.1021/ac201267k.

German NJ, Yoon H, Yusuf RZ, Murphy JP, Finley LWS, Laurent G, Haas W, Satterstrom FK, Guarnerio J, Zaganjor E, et al. (2016). PHD3 loss in cancer enables metabolic reliance on fatty acid oxidation via deactivation of ACC2. Mol. Cell 63, 1006–1020. 10.1016/j.molcel.2016.08.014. [PubMed: 27635760]

Gimenez-Cassina A, and Danial NN (2015). Regulation of mitochondrial nutrient and energy metabolism by BCL-2 family proteins. Trends Endocrinol. Metab 26, 165–175. 10.1016/j.tem.2015.02.004. [PubMed: 25748272]

Hanahan D, and Weinberg RA (2011). Hallmarks of cancer: the next generation. Cell 144, 646–674. 10.1016/j.cell.2011.02.013. [PubMed: 21376230]

Hormi M, Birsen R, Belhadj M, Huynh T, Cantero Aguilar L, Grignano E, Haddaoui L, Guillonneau F, Mayeux P, Hunault M, et al. (2020). Pairing MCL-1 inhibition with venetoclax improves therapeutic efficiency of BH3-mimetics in AML. Eur. J. Haematol 105, 588–596. 10.1111/ejh.13492. [PubMed: 32659848]

Huang CR, and Yang-Yen HF (2010). The fast-mobility isoform of mouse Mcl-1 is a mitochondrial matrix-localized protein with attenuated anti-apoptotic activity. FEBS Lett. 584, 3323–3330. 10.1016/j.febslet.2010.07.013. [PubMed: 20627101]

Huttlin EL, Jedrychowski MP, Elias JE, Goswami T, Rad R, Beausoleil SA, Villén J, Haas W, Sowa ME, and Gygi SP (2010). A tissue-specific atlas of mouse protein phosphorylation and expression. Cell 143, 1174–1189. 10.1016/j.cell.2010.12.001. [PubMed: 21183079]

Karbowski M, Norris KL, Cleland MM, Jeong SY, and Youle RJ (2006). Role of Bax and Bak in mitochondrial morphogenesis. Nature 443, 658–662. 10.1038/nature05111. [PubMed: 17035996]

Koss B, Morrison J, Perciavalle RM, Singh H, Rehg JE, Williams RT, and Opferman JT (2013). Requirement for antiapoptotic MCL-1 in the survival of BCR-ABL B-lineage acute lymphoblastic leukemia. Blood 122, 1587–1598. 10.1182/blood-2012-06-440230. [PubMed: 23881917]

Koss B, Ryan J, Budhraja A, Szarama K, Yang X, Bathina M, Cardone MH, Nikolovska-Coleska Z, Letai A, and Opferman JT (2016). Defining specificity and on-target activity of BH3-mimetics using engineered B-ALL cell lines. Oncotarget 7, 11500–11511. 10.18632/oncotarget.7204. [PubMed: 26862853]

Kotschy A, Szlavik Z, Murray J, Davidson J, Maragno AL, Le Toumelin-Braizat G, Chanrion M, Kelly GL, Gong JN, Moujalled DM, et al. (2016). The MCL1 inhibitor S63845 is tolerable and effective in diverse cancer models. Nature 538, 477–482. 10.1038/nature19830. [PubMed: 27760111]

Kuleshov MV, Jones MR, Rouillard AD, Fernandez NF, Duan Q, Wang Z, Koplev S, Jenkins SL, Jagodnik KM, Lachmann A, et al. (2016). Enrichr: a comprehensive gene set enrichment analysis web server 2016 update. Nucleic Acids Res. 44, W90–W97. 10.1093/nar/gkw377. [PubMed: 27141961]

Lee T, Christov PP, Shaw S, Tarr JC, Zhao B, Veerasamy N, Jeon KO, Mills JJ, Bian Z, Sensintaffar JL, et al. (2019). Discovery of potent myeloid cell leukemia-1 (Mcl-1) inhibitors that demonstrate in vivo activity in mouse xenograft models of human cancer. J. Med. Chem 62, 3971–3988. 10.1021/acs.jmedchem.8b01991. [PubMed: 30929420]

Li H, Ning S, Ghandi M, Kryukov GV, Gopal S, Deik A, Souza A, Pierce K, Keskula P, Hernandez D, et al. (2019). The landscape of cancer cell line metabolism. Nat. Med 25, 850–860. 10.1038/s41591-019-0404-8. [PubMed: 31068703]

Li J, Van Vranken JG, Pontano Vaites L, Schweppe DK, Huttlin EL, Etienne C, Nandhikonda P, Viner R, Robitaille AM, Thompson AH, et al. (2020). TMTpro reagents: a set of isobaric labeling mass tags enables simultaneous proteome-wide measurements across 16 samples. Nat. Methods 17, 399–404. 10.1038/s41592-020-0781-4. [PubMed: 32203386]

Liu X, Kim CN, Yang J, Jemmerson R, and Wang X (1996). Induction of apoptotic program in cell-free extracts: requirement for dATP and cytochrome c. Cell 86, 147–157. 10.1016/s0092-8674(00)80085-9. [PubMed: 8689682]

Love MI, Huber W, and Anders S (2014). Moderated estimation of fold change and dispersion for RNA-seq data with DESeq2. Genome Biol. 15, 550. 10.1186/s13059-014-0550-8. [PubMed: 25516281]

Ma Y, Temkin SM, Hawkridge AM, Guo C, Wang W, Wang XY, and Fang X (2018). Fatty acid oxidation: an emerging facet of metabolic transformation in cancer. Cancer Lett. 435, 92–100. 10.1016/j.canlet.2018.08.006.

Mamer O, Gravel SP, Choinière L, Chénard V, St-Pierre J, and Avizonis D (2013). The complete targeted profile of the organic acid intermediates of the citric acid cycle using a single stable isotope dilution analysis, sodium borodeuteride reduction and selected ion monitoring GC/MS. Metabolomics 9, 1019–1030. 10.1007/s11306-013-0521-1. [PubMed: 24348278]

McAlister GC, Huttlin EL, Haas W, Ting L, Jedrychowski MP, Rogers JC, Kuhn K, Pike I, Grothe RA, Blethrow JD, et al. (2012). Increasing the multiplexing capacity of TMTs using reporter ion isotopologues with isobaric masses. Anal. Chem 84, 7469–7478. 10.1021/ac301572t. [PubMed: 22880955]

McAlister GC, Nusinow DP, Jedrychowski MP, Wühr M, Huttlin EL, Erickson BK, Rad R, Haas W, and Gygi SP (2014). MultiNotch MS3 enables accurate, sensitive, and multiplexed detection of differential expression across cancer cell line proteomes. Anal. Chem 86, 7150–7158. 10.1021/ac502040v. [PubMed: 24927332]

McGuirk S, Gravel SP, Deblois G, Papadopoli DJ, Faubert B, Wegner A, Hiller K, Avizonis D, Akavia UD, Jones RG, et al. (2013). PGC-1alpha supports glutamine metabolism in breast cancer. Cancer Metab. 1, 22. 10.1186/2049-3002-1-22. [PubMed: 24304688]

Nanchen A, Fuhrer T, and Sauer U (2007). Determination of metabolic flux ratios from 13C-experiments and gas chromatography-mass spectrometry data: protocol and principles. Methods Mol. Biol 358, 177–197. 10.1007/978-1-59745-244-1_11. [PubMed: 17035687]

Navarrete-Perea J, Yu Q, Gygi SP, and Paulo JA (2018). Streamlined tandem mass tag (SL-TMT) protocol: an efficient strategy for quantitative (Phospho)proteome profiling using tandem mass tag-synchronous precursor selection-MS3. J. Proteome Res 17, 2226–2236. 10.1021/acs.jproteome.8b00217. [PubMed: 29734811]

Ni Chonghaile T, Sarosiek KA, Vo TT, Ryan JA, Tammareddi A, Moore VDG, Deng J, Anderson KC, Richardson P, Tai YT, et al. (2011). Pretreatment mitochondrial priming correlates with clinical response to cytotoxic chemotherapy. Science 334, 1129–1133. 10.1126/science.1206727. [PubMed: 22033517]

Oltvai ZN, Milliman CL, and Korsmeyer SJ (1993). Bcl-2 heterodimerizes in vivo with a conserved homolog, Bax, that accelerates programmed cell death. Cell 74, 609–619. 10.1016/0092-8674(93)90509-o.

Opferman JT, Iwasaki H, Ong CC, Suh H, Mizuno S.i., Akashi K, and Korsmeyer SJ (2005). Obligate role of anti-apoptotic MCL-1 in the survival of hematopoietic stem cells. Science 307, 1101–1104. 10.1126/science.1106114. [PubMed: 15718471]

Opferman JT, Letai A, Beard C, Sorcinelli MD, Ong CC, and Korsmeyer SJ (2003). Development and maintenance of B and T lymphocytes requires antiapoptotic MCL-1. Nature 426, 671–676. 10.1038/nature02067. [PubMed: 14668867]

Pascual G, Avgustinova A, Mejetta S, Martín M, Castellanos A, Attolini CSO, Berenguer A, Prats N, Toll A, Hueto JA, et al. (2017). Targeting metastasis-initiating cells through the fatty acid receptor CD36. Nature 541, 41–45. 10.1038/nature20791. [PubMed: 27974793]

Paulo JA, O'Connell JD, Everley RA, O'Brien J, Gygi MA, and Gygi SP (2016). Quantitative mass spectrometry-based multiplexing compares the abundance of 5000 S. cerevisiae proteins across 10 carbon sources. J. Proteomics 148, 85–93. 10.1016/j.jprot.2016.07.005. [PubMed: 27432472]

Perciavalle RM, Stewart DP, Koss B, Lynch J, Milasta S, Bathina M, Temirov J, Cleland MM, Pelletier S, Schuetz JD, et al. (2012). Anti-apoptotic MCL-1 localizes to the mitochondrial matrix and couples mitochondrial fusion to respiration. Nat. Cell Biol 14, 575–583. 10.1038/ncb2488. [PubMed: 22544066]

Raulien N, Friedrich K, Strobel S, Rubner S, Baumann S, von Bergen M, Körner A, Krueger M, Rossol M, and Wagner U (2017). Fatty acid oxidation compensates for lipopolysaccharide-induced Warburg effect in glucose-deprived monocytes. Front. Immunol 8, 609. 10.3389/fimmu.2017.00609. [PubMed: 28611773]

Reynolds JE, Yang T, Qian L, Jenkinson JD, Zhou P, Eastman A, and Craig RW (1994). Mcl-1, a member of the Bcl-2 family, delays apoptosis induced by c-Myc overexpression in Chinese hamster ovary cells. Cancer Res. 54, 6348–6352. [PubMed: 7987827]

Rinkenberger JL, Horning S, Klocke B, Roth K, and Korsmeyer SJ (2000). Mcl-1 deficiency results in peri-implantation embryonic lethality. Genes Dev. 14, 23–27. [PubMed: 10640272]

Rinkenberger JL, and Korsmeyer SJ (1997). Errors of homeostasis and deregulated apoptosis. Curr. Opin. Genet. Dev 7, 589–596. 10.1016/s0959-437x(97)80004-4. [PubMed: 9388773]

Roberts AW, Davids MS, Pagel JM, Kahl BS, Puvvada SD, Gerecitano JF, Kipps TJ, Anderson MA, Brown JR, Gressick L, et al. (2016). Targeting BCL2 with venetoclax in relapsed chronic lymphocytic leukemia. N. Engl. J. Med 374, 311–322. 10.1056/NEJMoa1513257. [PubMed: 26639348]

Samudio I, Harmancey R, Fiegl M, Kantarjian H, Konopleva M, Korchin B, Kaluarachchi K, Bornmann W, Duvvuri S, Taegtmeyer H, et al. (2010). Pharmacologic inhibition of fatty acid oxidation sensitizes human leukemia cells to apoptosis induction. J. Clin. Invest 120, 142–156. 10.1172/JCI38942. [PubMed: 20038799]

Sattler M, Liang H, Nettesheim D, Meadows RP, Harlan JE, Eberstadt M, Yoon HS, Shuker SB, Chang BS, Minn AJ, et al. (1997). Structure of Bcl-xL-Bak peptide complex: recognition between regulators of apoptosis. Science 275, 983–986. 10.1126/science.275.5302.983. [PubMed: 9020082]

Schweppe DK, Eng JK, Yu Q, Bailey D, Rad R, Navarrete-Perea J, Huttlin EL, Erickson BK, Paulo JA, and Gygi SP (2020). Full-featured, real-time database searching platform enables fast and accurate multiplexed quantitative proteomics. J. Proteome Res 19, 2026–2034. 10.1021/acs.jproteome.9b00860. [PubMed: 32126768]

Snaebjornsson MT, Janaki-Raman S, and Schulze A (2020). Greasing the Wheels of the cancer machine: the role of lipid metabolism in cancer. Cell Metab. 31, 62–76. 10.1016/j.cmet.2019.11.010. [PubMed: 31813823]

Souers AJ, Leverson JD, Boghaert ER, Ackler SL, Catron ND, Chen J, Dayton BD, Ding H, Enschede SH, Fairbrother WJ, et al. (2013). ABT-199, a potent and selective BCL-2 inhibitor, achieves antitumor activity while sparing platelets. Nat. Med 19, 202–208. 10.1038/nm.3048. [PubMed: 23291630]

Stevens BM, Jones CL, Pollyea DA, Culp-Hill R, D'Alessandro A, Winters A, Krug A, Abbott D, Goosman M, Pei S, et al. (2020). Fatty acid metabolism underlies venetoclax resistance in acute myeloid leukemia stem cells. Nat. Cancer 1, 1176–1187. 10.1038/s43018-020-00126-z. [PubMed: 33884374]

Tang Z, Kang B, Li C, Chen T, and Zhang Z (2019). GEPIA2: an enhanced web server for large-scale expression profiling and interactive analysis. Nucleic Acids Res. 47, W556–W560. 10.1093/nar/gkz430. [PubMed: 31114875]

Ting L, Rad R, Gygi SP, and Haas W (2011). MS3 eliminates ratio distortion in isobaric multiplexed quantitative proteomics. Nat. Methods 8, 937–940. 10.1038/nmeth.1714. [PubMed: 21963607]

Vander Heiden MG, and DeBerardinis RJ (2017). Understanding the intersections between metabolism and cancer biology. Cell 168, 657–669. 10.1016/j.cell.2016.12.039. [PubMed: 28187287]

Walensky LD, and Gavathiotis E (2011). BAX unleashed: the biochemical transformation of an inactive cytosolic monomer into a toxic mitochondrial pore. Trends Biochem. Sci 36, 642–652. 10.1016/j.tibs.2011.08.009. [PubMed: 21978892]

Wanders RJ, Vreken P, den Boer ME, Wijburg FA, van Gennip AH, and IJlst L (1999). Disorders of mitochondrial fatty acyl-CoA beta-oxidation. J. Inherit. Metab. Dis 22, 442–487. 10.1023/a:1005504223140. [PubMed: 10407780]

Wang H, Guo M, Wei H, and Chen Y (2021). Targeting MCL-1 in cancer: current status and perspectives. J. Hematol. Oncol 14, 67. 10.1186/s13045-021-01079-1. [PubMed: 33883020]

Wang X, Bathina M, Lynch J, Koss B, Calabrese C, Frase S, Schuetz JD, Rehg JE, and Opferman JT (2013). Deletion of MCL-1 causes lethal cardiac failure and mitochondrial dysfunction. Genes Dev. 27, 1351–1364. 10.1101/gad.215855.113. [PubMed: 23788622]

Wang Y, Yang F, Gritsenko MA, Wang Y, Clauss T, Liu T, Shen Y, Monroe ME, Lopez-Ferrer D, Reno T, et al. (2011). Reversed-phase chromatography with multiple fraction concatenation strategy for proteome profiling of human MCF10A cells. Proteomics 11, 2019–2026. 10.1002/pmic.201000722. [PubMed: 21500348]

Wei G, Twomey D, Lamb J, Schlis K, Agarwal J, Stam RW, Opferman JT, Sallan SE, den Boer ML, Pieters R, et al. (2006). Gene expression-based chemical genomics identifies rapamycin as a modulator of MCL1 and glucocorticoid resistance. Cancer Cell 10, 331–342. 10.1016/j.ccr.2006.09.006. [PubMed: 17010674]

Wei MC, Lindsten T, Mootha VK, Weiler S, Gross A, Ashiya M, Thompson CB, and Korsmeyer SJ (2000). tBID, a membrane-targeted death ligand, oligomerizes BAK to release cytochrome c. Genes Dev. 14, 2060–2071. [PubMed: 10950869]

Wuillème-Toumi S, Robillard N, Gomez P, Moreau P, Le Gouill S, Avet-Loiseau H, Harousseau JL, Amiot M, and Bataille R (2005). Mcl-1 is overexpressed in multiple myeloma and associated with relapse and shorter survival. Leukemia 19, 1248–1252. 10.1038/sj.leu.2403784. [PubMed: 15902294]

Xu HE, Stanley TB, Montana VG, Lambert MH, Shearer BG, Cobb JE, McKee DD, Galardi CM, Plunket KD, Nolte RT, et al. (2002). Structural basis for antagonist-mediated recruitment of nuclear co-repressors by PPARalpha. Nature 415, 813–817. 10.1038/415813a. [PubMed: 11845213]

Yecies D, Carlson NE, Deng J, and Letai A (2010). Acquired resistance to ABT-737 in lymphoma cells that up-regulate MCL-1 and BFL-1. Blood 115, 3304–3313. 10.1182/blood-2009-07-233304. [PubMed: 20197552]

Highlights

- MCL-1 controls fatty acid oxidation independent of its anti-apoptotic function

- Genetic deletion of *Mcl-1* induces global downregulation of the FAO pathway

- MCL-1-driven hematologic cancer cells are dependent on FAO as a fuel source

- MCL-1-dependent cancer cells are selectively susceptible to FAO inhibitors
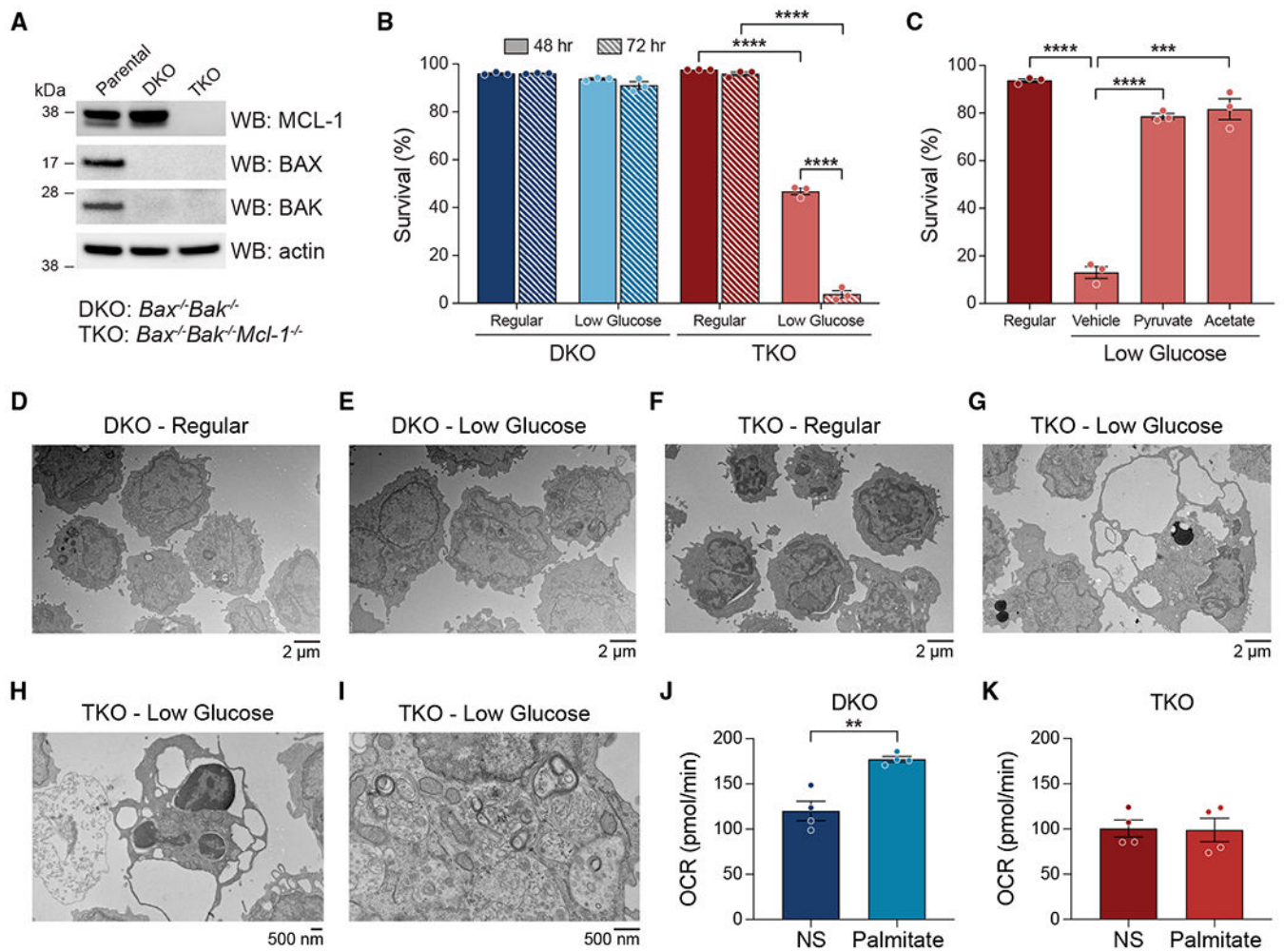
Figure 1. Genetic deletion of *Mcl-1* in the absence of BAX/BAK confers sensitivity to glucose deprivation

(A) Western blot of MCL-1, BAX, BAK, and actin in parental, DKO, and TKO B-ALL cells.

(B) Comparative survival of DKO and TKO cells in regular medium and upon glucose deprivation, as assessed by propidium iodide staining and flow cytometry at 48 and 72 h. Data are mean ± SEM of three biological replicates. Statistical significance was calculated using two-tailed Student's t test; *p < 0.05, **p < 0.01, ***p < 0.001, ****p < 0.0001.

(C) Comparative survival of TKO cells in regular medium and upon glucose deprivation with addition of vehicle, sodium pyruvate, or sodium acetate to the medium, as assessed by propidium iodide staining and flow cytometry at 72 h. Data are mean ± SEM of three biological replicates. Statistical significance was calculated using two-tailed Student's t test; *p < 0.05, **p < 0.01, ***p < 0.001, ****p < 0.0001.

(D and E) Representative electron microscopy (EM) images of DKO cells in regular medium (D) and upon glucose deprivation (E) for 48 h.

(F–I) Representative EM images of TKO cells in regular medium (F) and upon glucose deprivation (G–I) for 48 h.

(J and K) OCR of DKO (J) and TKO (K) cells in the presence and absence of added palmitate, as measured by Seahorse analysis. NS, no substrate. Data are mean ± SEM for

experiments performed in technical quadruplicate and repeated twice with similar results. Statistical significance was calculated using two-tailed Student's t test; *p < 0.05, **p < 0.01, ***p < 0.001, ****p < 0.0001.
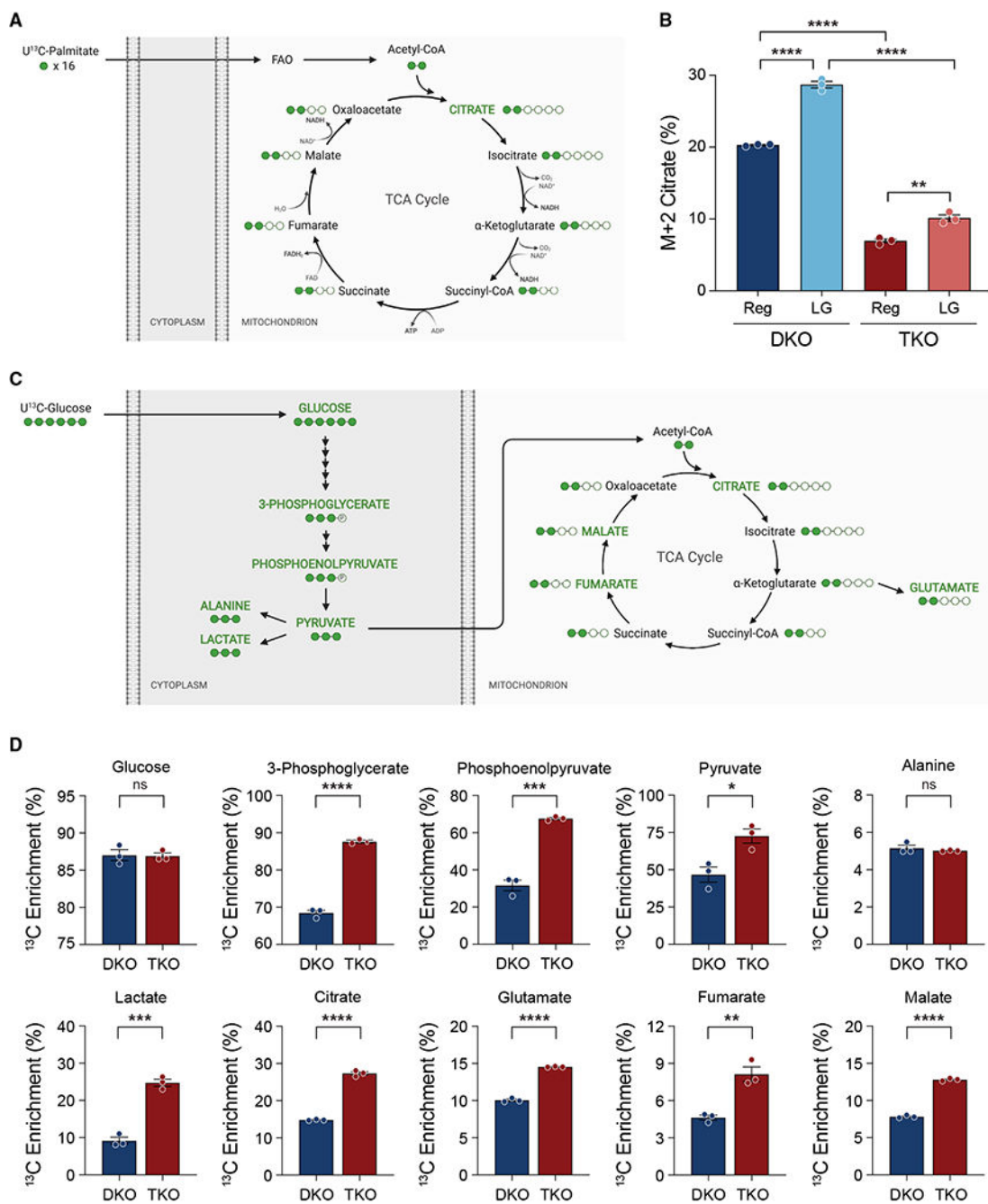
Figure 2. B-ALL cells lacking BAX/BAK undergo metabolic rewiring from lipid to glucose utilization upon genetic deletion of *Mcl-1*

(A) Schematic of $U^{13}C$-palmitate tracing analysis, depicting the number of citrate carbons derived from palmitate in the first round of the TCA cycle (M+2 citrate).

(B) Percentage of M+2 citrate in response to $U^{13}C$-palmitate tracing in DKO and TKO cells cultured in regular (Reg) or low-glucose (LG) medium for 24 h. Data are mean ± SEM for experiments performed in technical triplicate and repeated twice with similar results. Statistical significance was calculated using two-tailed Student's t test; *p < 0.05, **p < 0.01, ***p < 0.001, ****p < 0.0001.

(C) Schematic of U^{13}C-glucose tracing analysis, depicting the number of carbons labeled in glycolytic and TCA cycle metabolites.

(D) Percentage of ^{13}C-labeled metabolites in response to U^{13}C-glucose tracing for DKO and TKO cells cultured in regular medium for 24 h. Data are mean ± SEM for experiments performed in technical triplicate and repeated twice with similar results. Statistical significance was calculated using the two-tailed Student's t test; $*p < 0.05$, $**p < 0.01$, $***p < 0.001$, $****p < 0.0001$.

See also Figure S1.
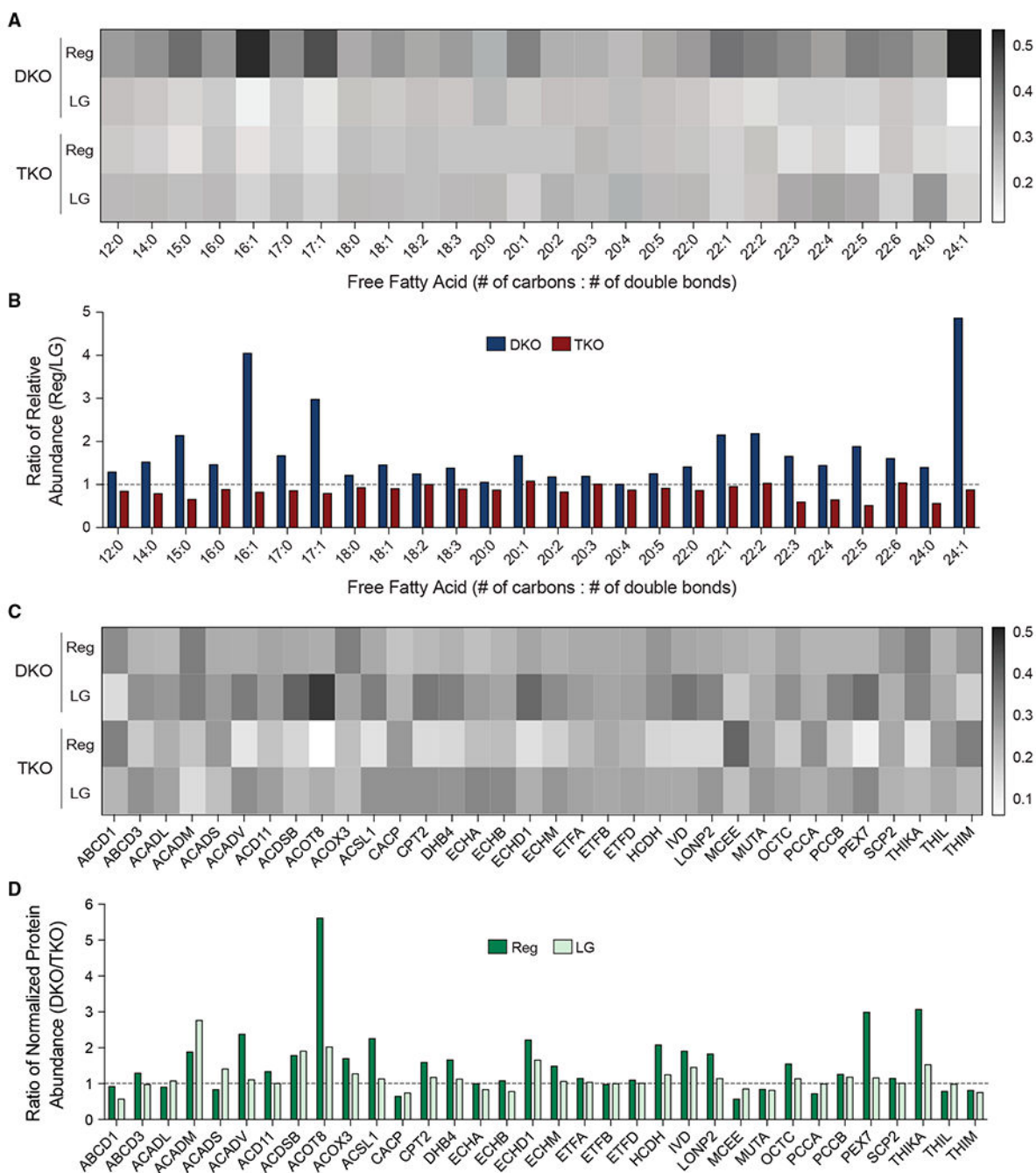
Figure 3. Comparative levels of fatty acids and FAO proteins in DKO and TKO cells cultured in regular and low-glucose media

(A) Heatmap depiction of FFA levels in DKO and TKO cells cultured in regular medium and upon glucose deprivation for 24 h. Reg, regular medium; LG, low-glucose medium. Data are the mean of two (DKO/Reg) or three (DKO/LG, TKO/Reg, TKO/LG) technical replicates.

(B) Ratio of the relative abundance of FFAs in DKO and TKO cells cultured in regular versus low-glucose medium for 24 h. Data are the mean of two (DKO/Reg) or three (DKO/LG, TKO/Reg, TKO/LG) technical replicates.

(C) Heatmap depiction of FAO protein levels in DKO and TKO cells cultured in regular medium and upon glucose deprivation for 24 h. Data are the mean of two (DKO/Reg, TKO/Reg) or three (DKO/LG, TKO/LG) technical replicates.

(D) Ratio of the normalized abundance of the indicated FAO proteins in DKO versus TKO cells cultured in regular medium and upon glucose deprivation for 24 h. Data are the mean of two (DKO/Reg, TKO/Reg) or three (DKO/LG, TKO/LG) technical replicates.

See also Figure S2.
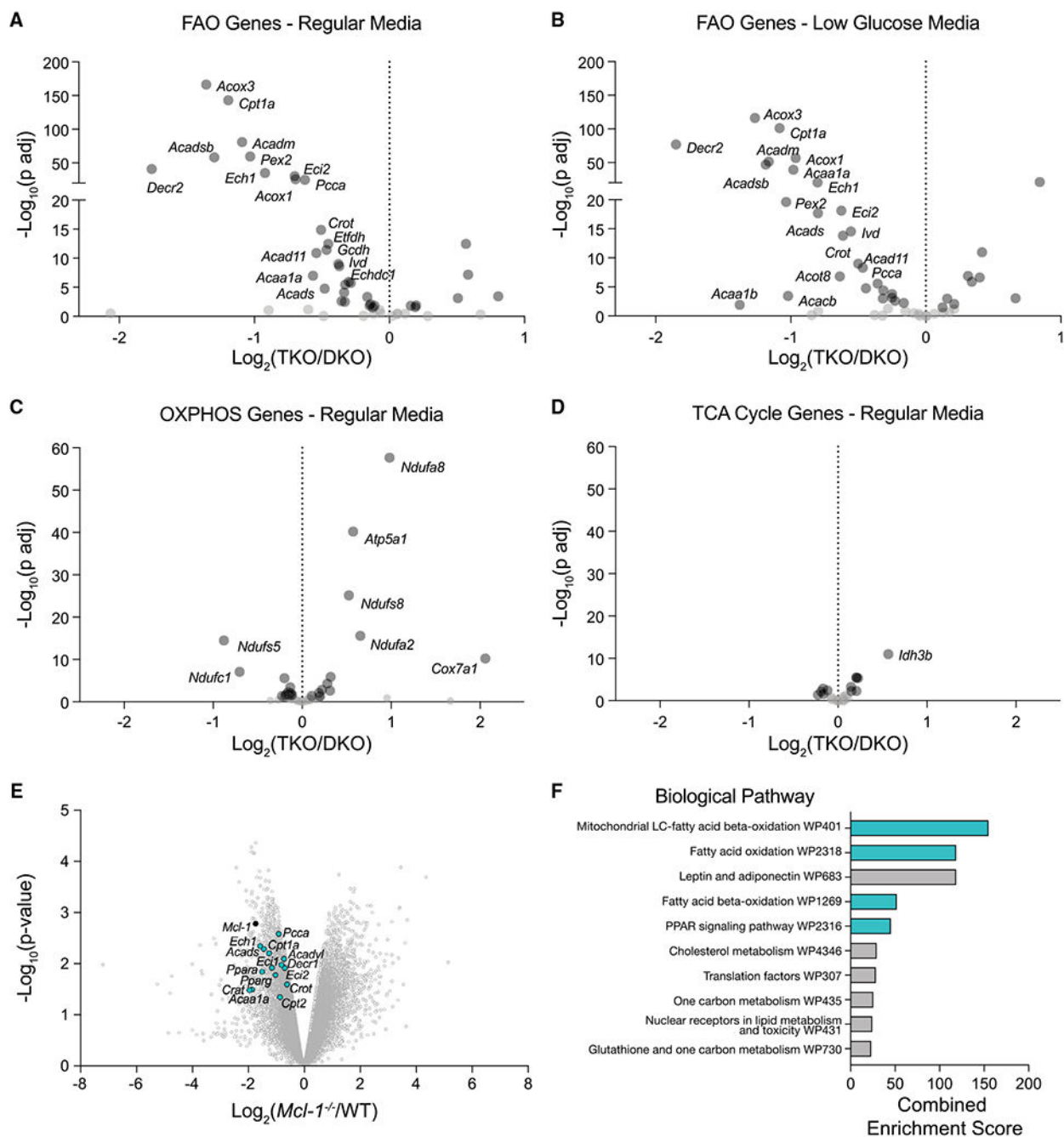
Figure 4. Selective downregulation of FAO gene sets upon genetic deletion of *Mcl-1* in murine B-ALL cells and liver tissue

(A and B) Volcano plot depictions of comparative FAO gene expression in DKO and TKO cells cultured in regular (A) and low-glucose (B) media for 24 h. Data are the mean of three technical replicates. Genes with statistically significant changes based on the Wald test, with correction for multiple hypothesis testing using the Benjamini-Hochberg method, are shown in dark gray.

(C and D) Volcano plot depictions of comparative expression changes of OXPHOS (C) and TCA cycle (D) gene sets in DKO and TKO cells cultured in regular medium. Data are the

mean of three technical replicates. Genes with statistically significant changes based on the Wald test, with correction for multiple hypothesis testing using the Benjamini-Hochberg method, are shown in dark gray.

(E) Volcano plot depiction of comparative gene expression changes in wild-type (WT) versus *Mcl-1*$^{-/-}$ murine livers, as determined by RNA-seq. *Mcl-1* and FAO-related genes are shown in black and teal, respectively.

(F) Downregulation of FAO and PPAR signaling pathway gene sets (teal) upon deletion of *Mcl-1* in murine liver.

See also Figures S3 and S4.
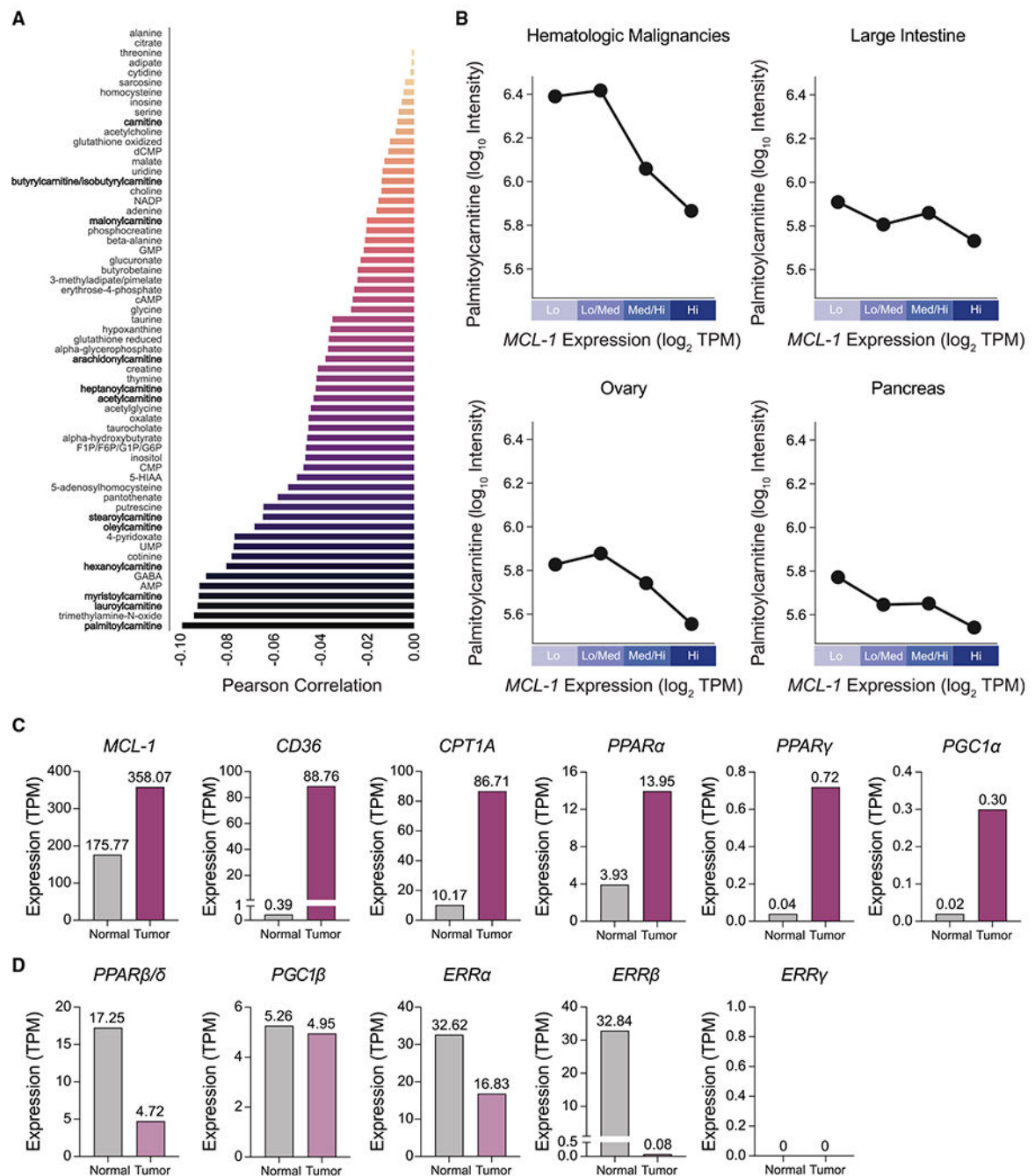
Figure 5. Correlation of *MCL-1* expression with changes in metabolites and FAO gene expression in human cancer

(A) Ranked list of metabolites that negatively correlate with *MCL-1* expression across the CCLE. The most negatively correlated species are located at the bottom of the plot, with carnitine species highlighted in bold.

(B) Inverse correlation of palmitoylcarnitine levels with *MCL-1* expression across four exemplary classes of human cancer.

(C and D) Comparative gene expression analysis of *MCL-1* and key FAO-related genes in human AML (TCGA) versus normal bone marrow (GTEx), revealing relative co-

upregulation of *MCL-1, CD36, CPT1A, PPARα, PPARγ*, and *PGC1α* in AML(C) and no change (*PGC1β* and *ERRγ*) or relative downregulation (*PPARβ/δ*, *ERRα*, and *ERRβ*) (D).
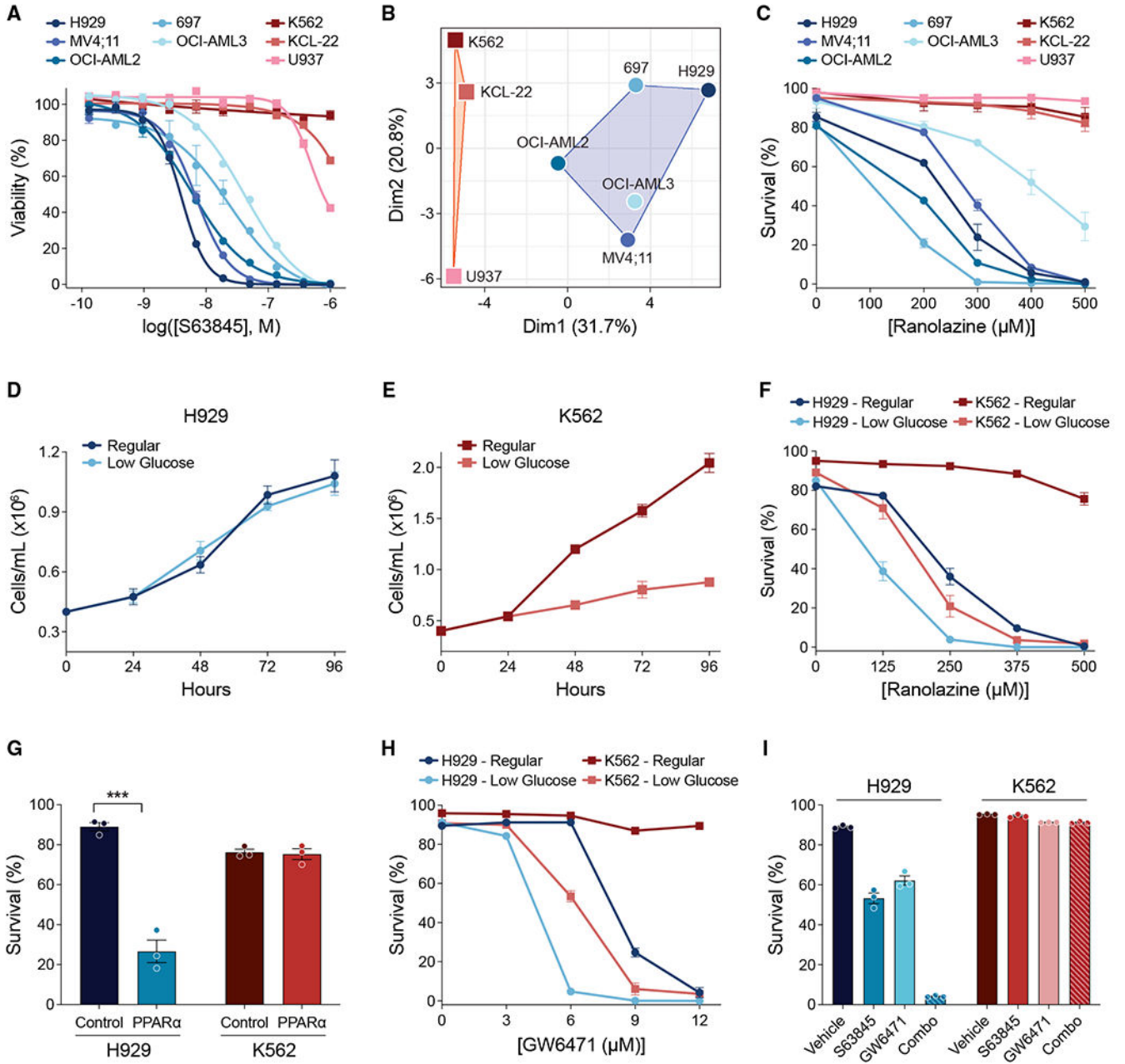
Figure 6. Selective sensitivity of MCL-1-dependent cancer cells to FAO inhibition

(A) Cell viability of hematologic cancer cell lines in response to treatment with the indicated doses of S63845 for 48 h, as assessed by CellTiter-Glo. Data are mean ± SEM for experiments performed in technical triplicate and repeated twice with similar results.

(B) Clustering analysis of hematologic cancer cells using the k-means algorithm based on expression of an FAO gene set.

(C) Hematologic cancer cell survival in response to treatment with the indicated doses of ranolazine for 96 h, as assessed by propidium iodide staining and flow cytometry. Data are mean ± SEM of three biological replicates.

(D and E) Proliferation of H929 (D) and K562 (E) cells cultured in regular or low-glucose medium, as measured every 24 h for 96 h. Data are mean ± SEM for experiments performed in technical triplicate and repeated twice with similar results.

(F) Survival of H929 and K562 cells cultured in regular or low-glucose medium and treated with the indicated doses of ranolazine for 96 h, as assessed by propidium iodide staining and flow cytometry. Data are mean ± SEM of three biological replicates.

(G) Survival of H929 and K562 cells cultured in regular medium and treated with a PPARα small interfering RNA (siRNA) pool or non-targeting control for 96 h, as determined by propidium iodide staining and flow cytometry. Data are mean ± SEM of three biological replicates. Statistical significance was calculated using two-tailed Student's t test; $*p < 0.05$, $**p < 0.01$, $***p < 0.001$, $****p < 0.0001$.

(H) Survival of H929 and K562 cells in response to treatment with the indicated doses of GW6471 in regular and low-glucose media for 96 h, as assessed by propidium iodide staining and flow cytometry. Data are mean ± SEM of three biological replicates.

(I) Survival of H929 and K562 cells in response to treatment with S63845 (5 nM), GW6471 (8 μM), or the combination for 96 h, as assessed by propidium iodide staining and flow cytometry. Data are mean ± SEM of three biological replicates.

See also Figures S5 and S6.

KEY RESOURCES TABLE

REAGENT or RESOURCE	SOURCE	IDENTIFIER
Antibodies		
Rabbit polyclonal anti-MCL-1	Rockland Immunochemicals	Cat #600-401-394, RRID: AB_2266446
Rabbit monoclonal anti-BAX	Cell Signaling Technology	Cat #14796, RRID: AB_2716251
Rabbit monoclonal anti-BAK	Cell Signaling Technology	Cat #12105, RRID: AB_2716685
Mouse monoclonal anti-BCL-2 (HRP)	Santa Cruz Biotechnology	Cat #sc-509 HRP, RRID: AB_626733
Rabbit monoclonal anti-actin (HRP)	Cell Signaling Technology	Cat #5125, RRID: AB_1903890
Chemicals, peptides, and recombinant proteins		
Complete protease inhibitor cocktail tablets	Sigma-Aldrich	Cat #05056489001
Propidium iodide	Thermo Fisher Scientific	Cat #P3566
Sodium pyruvate	Thermo Fisher Scientific	Cat #11360070
Sodium acetate	Thermo Fisher Scientific	Cat #R1181
Cell-Tak	Corning	Cat #354240
$U^{13}C$-palmitate	Cambridge Isotope Laboratories	Cat #CLM-409
$1^{13}C$-hexanoate	Cambridge Isotope Laboratories	Cat #CLM-3519
$U^{13}C$-glucose	Cambridge Isotope Laboratories	Cat #CLM-481
Methoxyamine	Sigma-Aldrich	Cat #226904
Pyridine	Sigma-Aldrich	Cat #270970
MTBSTFA	Sigma-Aldrich	Cat #394882
S63845	Selleck Chemicals	Cat #S8383
ABT-199	Selleck Chemicals	Cat #S8048
Ranolazine dihydrochloride	Selleck Chemicals	Cat #S1425
GW6471	Selleck Chemicals	Cat #S2798
Critical commercial assays		
MycoAlert Mycoplasma Detection Kit	Lonza Biologics	Cat #LT07-218
Pierce BCA Protein Assay Kit	Thermo Fisher Scientific	Cat #23225
RNeasy Mini Kit	Qiagen	Cat #74124
Kapa mRNA HyperPrep Strand Specific Sample Preparation Kit	Roche	Cat # KK8580
CellTiter-Glo© Luminescent Cell Viability Assay	Promega	Cat #G7571
Deposited data		
Metabolomic Data	This paper	MetaboLights: MTBLS4225
Proteomic Data	This paper	ProteomeXchange via PRIDE: PXD031364
RNA-seq Data	This paper	NCBI GEO: GSE196136
Experimental models: Cell lines		
Parental p185$^+$Arf$^{-/-}$ B-ALL	Koss et al., 2013	N/A
Bax$^{-/-}$Bak$^{-/-}$ (DKO) p185$^+$Arf$^{-/-}$ B-ALL	Koss et al., 2013	N/A
Bax$^{-/-}$Bak$^{-/-}$Mcl-1$^{-/-}$ (TKO) p185$^+$Arf$^{-/-}$ B-ALL	Koss et al., 2013	N/A

REAGENT or RESOURCE	SOURCE	IDENTIFIER
Bax⁻/⁻*Bak*⁻/⁻*Mcl-1*⁻/⁻*hMCL-1* (TKO + MCL-1) p185⁺*Arf*⁺/⁻ B-ALL	This paper	N/A
Mcl-1⁻/⁻*hBCL-2^{OE}* (BCL-2^{OE}) p185⁺*Arf*⁺/⁻ B-ALL	Koss et al., 2013	N/A
Mcl-1⁻/⁻*hMCL-1^{OE}* (MCL-1^{OE}) p185⁺*Arf*⁺/⁻ B-ALL	Koss et al., 2013	N/A
H929	ATCC	Cat #CRL-9068
MV4;11	ATCC	Cat #CRL-9591
OCI-AML2	DSMZ	Cat #ACC 99
697	DSMZ	Cat #ACC 42
OCI-AML3	DSMZ	Cat #ACC 582
U937	ATCC	Cat #CRL-1593.2
KCL-22	DSMZ	Cat #ACC 519
K562	ATCC	Cat #CCL-243
Oligonucleotides		
Accell non-targeting control siRNA pool	Horizon Discovery	Cat #D-001910-10-05
Accell human PPARα siRNA pool	Horizon Discovery	Cat #E-003434-00-0005
Software and algorithms		
Prism v9	GraphPad Software	https://www.graphpad.com/scientific-software/prism/
Seahorse Wave Software	Agilent Technologies	https://www.agilent.com/en/product/cell-analysis/real-time-cell-metabolic-analysis/xf-software/seahorse-wave-desktop-software-740897
MassHunter Quantitative Analysis	Agilent Technologies	https://www.agilent.com/en/product/software-informatics/mass-spectrometry-software/data-analysis/quantitative-analysis
Analyst 1.6.3	Sciex	https://sciex.com/products/software/analyst-software
Bioinformatics, Statistics, Database, and Parallel Computing Toolboxes	MATLAB	https://www.mathworks.com/products/matlab.html?s_tid=hp_products_matlab
Comet	Eng et al., 2013	https://uwpr.github.io/Comet/
STAR v2.7.3a	Dobin et al., 2013	https://github.com/alexdobin/STAR
DESeq2 v1.22.1	Love et al., 2014	https://bioconductor.org/packages/release/bioc/html/DESeq2.html
VIPER	Cornwell et al., 2018	https://github.com/hanfeisun/viper-rnaseq
GEO2R	Barrett_et_al_2013	https://www.ncbi.nlm.nih.gov/geo/geo2r/
Enrichr	Chen et al., 2013	https://maayanlab.cloud/Enrichr/
GEPIA2	Tang et al., 2019	http://gepia2.cancer-pku.cn/#index
Other		
RPMI 1640	Thermo Fisher Scientific	Cat #21870-076
RPMI 1640, no glucose	Thermo Fisher Scientific	Cat #11879-020
Fetal Bovine Serum	GeminiBio	Cat #100-106, Lot #A33H00L